BEYOND-THE-HORIZON VHF COMMUNICATION USING MAN-MADE IONOSPHERIC SCATTERERS

Roy A. Sasselli, et al

Barry Research Corporation

Prepared for:

Defense Advanced Research Projects Agency
Rome Air Development Center

December 1974

UNCLASSIFIED

SECURITY CLASSIFICATION OF THIS PAGE (When Data Entered)

REPORT DOCUMENTATION PAGE		READ INSTRUCTIONS BEFORE COMPLETING FORM
1. REPORT NUMBER RADC-TR-74-316	2. GOVT ACCESSION NO.	3. RECIPIENT'S CATALOG NUMBER AD/A003641
4. TITLE (and Subtitle) Beyond-The-Horizon VHF Communication Using Man-Made Ionospheric Scatterers		5. TYPE OF REPORT & PERIOD COVERED Final Technical Report May 1973 - July 1974 6. PERFORMING ORG. REPORT NUMBER
7. AUTHOR(s) Roy A. Sasselli John F. McLaughlin		8. CONTRACT OR GRANT NUMBER(s) F30602-73-C-0263
9. PERFORMING ORGANIZATION NAME AND ADDRESS Barry Research Corporation 1530 Page Mill Road Palo Alto CA 94304		10. PROGRAM ELEMENT, PROJECT, TASK AREA & WORK UNIT NUMBERS 62301E 20791101
11. CONTROLLING OFFICE NAME AND ADDRESS Defense Advanced Research Projects Agency 1400 Wilson Blvd Arlington VA 22209		12. REPORT DATE December 1974 13. NUMBER OF PAGES 91
14. MONITORING AGENCY NAME & ADDRESS(if different from Controlling Office) Rome Air Development Center (OCSE) ATTN: Richard A. Schneible Griffiss AFB NY 13441		15. SECURITY CLASS. (of this report) UNCLASSIFIED 15a. DECLASSIFICATION/DOWNGRADING SCHEDULE NA

16. DISTRIBUTION STATEMENT (of this Report)

Approved for public release. Distribution unlimited.

17. DISTRIBUTION STATEMENT (of the abstract entered in Block 20, if different from Report)

Approved for public release. Distribution unlimited.

18. SUPPLEMENTARY NOTES

Monitored by: Richard A. Schneible/RADC (OCSE)
Griffiss AFB NY 13441
AC 315 330-3085

19. KEY WORDS (Continue on reverse side if necessary and identify by block number)

Communications
Special Techniques
Ionospheric Scatter Propagation
Ionospheric Modification

20. ABSTRACT (Continue on reverse side if necessary and identify by block number)

The ARPA sponsored IVORY CORAL program demonstrated that an ionospheric disturbance can be created by irradiating the ionosphere at vertical incidence with high power radio signals at a frequency corresponding to the ionospheric plasma frequency. At HF and VHF, the disturbance appears as a cloud of electron density irregularities which scatters incident signals at frequencies far higher than those which would normally be ionospherically reflected. This report summarizes the design of a communications circuit using the man-

DD FORM 1 JAN 73 1473 EDITION OF 1 NOV 65 IS OBSOLETE

UNCLASSIFIED

SECURITY CLASSIFICATION OF THIS PAGE (When Data Entered)

made ionospheric scatters and the characteristics of VHF signals propagated over such a circuit. It represents a compilation of experimental data obtained during field exercises in which communications were established between terminals separated 1400 km and 2200 km. The report summarizes the requirements of an ionospheric heater and describes the characteristics of the disturbances itself. These characteristics include observed radar cross section as a function of time of day, amount of heater power, and heater modulation. The observed characteristics of a scattered signal are shown for frequencies in the 30-80 MHz range. These include amplitude fading vs frequency and time of day, fading distribution, fading correlation bandwidth, and signal power spectrum vs frequency and time of day.

BEYOND-THE-HORIZON VHF COMMUNICATION USING MAN-MADE IONOSPHERIC SCATTERERS

Roy A. Sasselli
John F. McLaughlin

Contractor: Barry Research Corporation
Contract Number: F30602-73-C-0263
Effective Date of Contract: May 1973
Contract Expiration Date: July 1974
Amount of Contract: $253,958.00
Program Code Number: 2E20
Period Covered: May 1973 - July 1974

Principal Investigator: Dr. George H. Barry
Phone: 415 493-6800

Project Engineer: Vincent J. Coyne
Phone: 315 330-3141

Contract Engineer: Richard A. Schneible
Phone: 315 330-3085

This research was supported by the Defense Advanced Research Projects Agency of the Department of Defense and was monitored by Richard A. Schneible, RADC (OCSE), GAFB NY 13441 under Contract F30602-73-C-0263, Job Order No. 20791101.

This report has been reviewed by the RADC Information Office (OI), and is releasable to the National Technical Information Service (NTIS).

This technical report has been reviewed and is approved.

Richard A. Schreibold

RADC Project Engineer

TABLE OF CONTENTS

TECHNICAL REPORT SUMMARY

The ARPA-sponsored IVORY CORAL program demonstrated that an ionospheric disturbance can be created by irradiating the ionosphere at vertical incidence with high power radio signals at a frequency corresponding to the ionospheric plasma frequency. At HF and at VHF, the disturbance appears as a cloud of electron density irregularities which scatters incident signals at frequencies far higher than those which would normally be ionospherically reflected. Cloud cross sections of 10^5 to 10^7 m^2 have been observed on frequencies from 10 to 100 MHz, however, the cloud represents a very weak and aspect sensitive scatterer, so that large cross sections are available only when certain geometric restrictions are met.

This report summarizes the design of a communications circuit using the man-made ionospheric scatterers and the characteristics of VHF signals propagated over such a circuit. It represents a compilation of experimental data obtained during field exercises in which communications were established between terminals separated 1400 km and 2200 km. The scattering cloud was located 1000-1200 km from both transmitter and receiver terminals.

The report summarizes the requirements of an ionospheric heater and describes the characteristics of the disturbance itself. These characteristics include observed radar cross section as a function of time of day, amount of heater radiated power, and heater modulation.

The observed characteristics of a scattered signal are shown for frequencies in the 30-80 MHz range. These include amplitude fading vs frequency and time of day, fading distribution, fading correlation bandwidth, and signal power spectrum vs frequency and time of day.

Finally, the effects of signal scatter requirements on communication system design are summarized including site location requirements, system energy requirements, and antenna design considerations. The effects of signal fading on communication reliability are also presented along with data on the benefits derived from various diversity reception techniques.

Section 1
INTRODUCTION

The following report describes a technique of achieving beyond-the-horizon VHF signal transmission by scatter from a man-made ionospheric disturbance. The characteristics of the required ionospheric modification facility are described in Section 2. Section 3 summarizes the observed effects on over-the-horizon VHF signals obliquely scattered off the ionospheric disturbance. Finally, Section 4 summarizes the major characteristics of a VHF communications link utilizing the scatter technique.

1.1 HISTORY OF IONOSPHERIC MODIFICATION STUDIES

A theoretical discussion of modifying the F-region of the ionosphere by heating it at a plasma resonance via deviative absorption of RF energy from a controlled ground-based facility was first presented by Ginzburg and Gurevich in a U.S.S.R. publication (Reference 1) in 1960. Subsequent theoretical analyses in Russia and the United States led to experimental efforts to heat the ionosphere using a specially constructed transmitter facility built and operated by the Institute for Telecommunications Sciences (ITS) at a site near Platteville, Colorado.

The early experimental effort, initiated in April 1970, grew into the IVORY CORAL program sponsored by the Strategic Technology Office of the Advanced Research Projects Agency. The IVORY CORAL program combined theoretical studies and field experiments over a four-year period. The results of this program are presented in a series of reports published by Stanford Research Institute (References 2-7) and an overall summary compiled by Vanderlind of Battelle Institute (Reference 8).

An ARPA-sponsored program to examine the applications of ionospheric heating technology began in 1971. This effort included systems studies and a field program demonstrating long-range VHF communication (Project STEEP CLIFF). Results of the systems studies are presented in Reference 9. The initial STEEP CLIFF I experimental results are described in Reference 10. These experiments and STEEP CLIFF II field test program provide the principal data base for the information in the following sections. The STEEP CLIFF programs are described in Appendix A.

1.2 EFFECTS OF IONOSPHERIC HEATING

During the course of the IVORY CORAL program, heating of the ionosphere has been accomplished by two vertically-radiating transmitter facilities: the ITS Platteville facility and the Arecibo Ionospheric Observatory (AIO) in Puerto Rico. The Platteville facility uses ten power amplifiers each connected to elements of crossed dipole arrays, while the AIO installation uses a single 150-kW power amplifier feeding the 1000-ft diameter AIO dish antenna. The experimental results of this report are based entirely upon the disturbances generated by the Platteville facility and, accordingly, it is discussed in Section 2 of this report as a model heater facility.

Heating the ionosphere results in five main effects* observable by ground-based measuring equipment:

(1) artificial spread-F which is observable by vertical-or oblique-incidence ionosondes transmitting through the disturbed region and which produces scintillations of VHF and UHF satellite transmissions;

(2) scatter of HF, VHF and UHF signals by irregularities in the heated F-region aligned with the geomagnetic field;

*For detailed discussion of the effects, the reader is referred to References 6 and 8.

(3) plasma-wave scatter, producing RF echoes shifted above and below the radar frequency by approximately the heater frequency;

(4) ion acoustic-wave scatter producing an enhancement in the incoherent-backscatter spectrum; and

(5) optical (airglow) enhancements observable on occasion at several wavelengths including 6300Å, 5577Å, and 1.27 microns.

Of the various heating effects, the second -- field-aligned scatter -- has the most obvious potential applications. Plasma-wave and ion-acoustic wave scatter yield radar cross-sections under 10^3 m^2 and are considered too weak to be of practical importance; however, the field-aligned scattering region appears as a VHF radar target which is often as large as 10^6 m^2. The remainder of this report will therefore concern itself solely with field-aligned scatter.

1.3 FIELD-ALIGNED SCATTER

HF heating of the F-region ionosphere appears to produce electron density irregularities aligned with the geomagnetic field in a disturbance region both above and below the heater RF reflection height (the altitude at which the plasma frequency is equal to the frequency of a vertically-incident HF heater signal). This is shown in Figure 1-1 taken from Reference 6. The disturbance region can be thought of as having a Gaussian envelope with a locus of 1/e (-4 dB) points roughly forming a horizontal disc 100 km in diameter and 15 km thick centered at the heater reflection altitude. Distributed throughout the disturbed region are long, thin, field-aligned irregularities which can again be thought of in terms of Gaussian envelopes 0.1-0.5 meters thick and 10 km long. The rms density fluctuation producing these irregularities is estimated at about 1 percent.

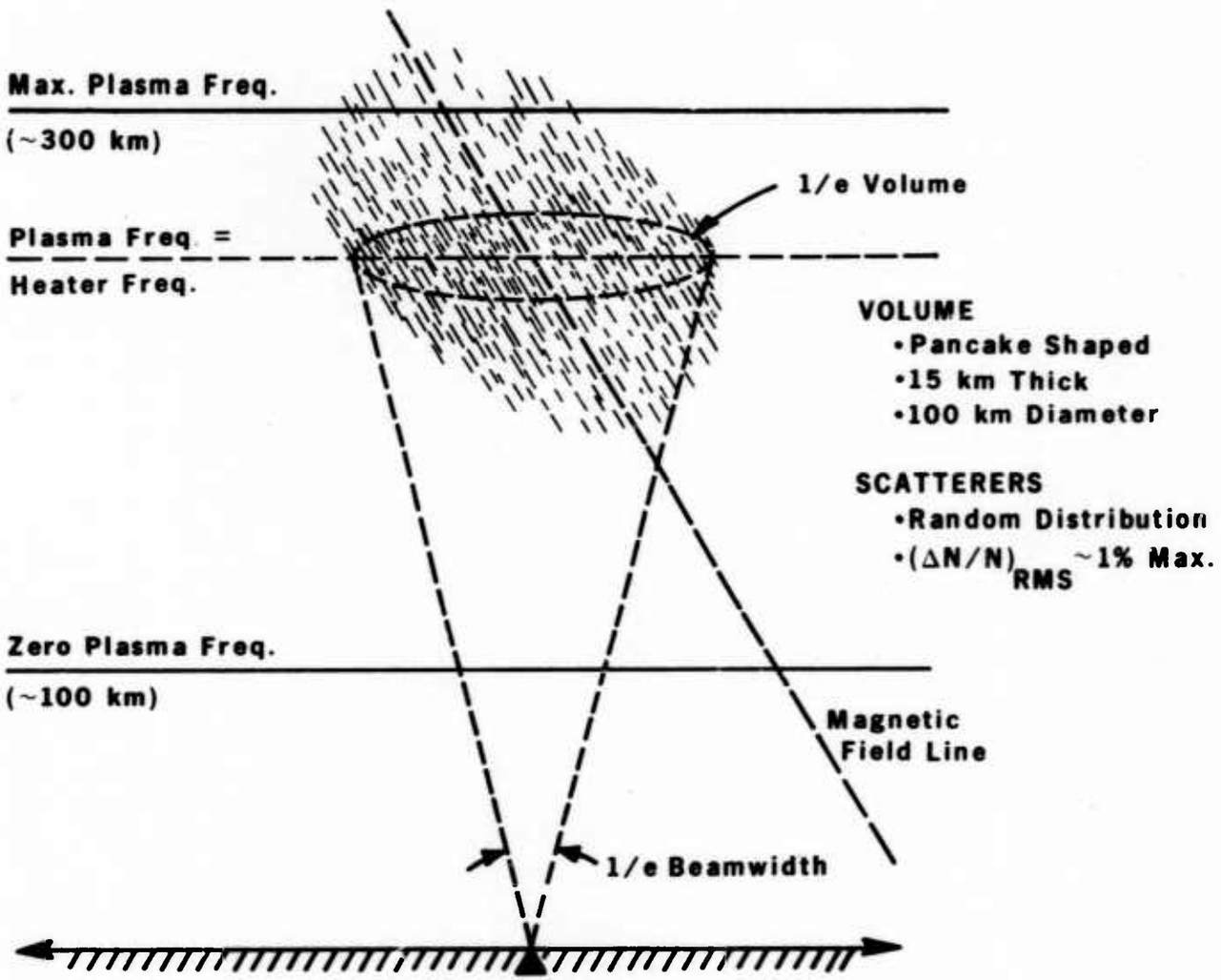

Figure 1-1. Physical Model of the Disturbed Ionospheric Volume.

The individual irregularities within the disturbed region can be visualized as acting like long, thin cylinders aligned with the geomagnetic field. RF energy scatters off each cylinder much as a beam of light would be scattered by a shiny metal rod. When the illumination is perpendicular to the axis of the cylinder, the cylinder will scatter energy throughout the plane normal to the cylinder and containing the illuminating ray. Thus, some energy will be scattered back in the direction of the illuminator and can be received at the same location from which it was transmitted, as in the case of a monostatic radar. Obviously, the cylinder must be perpendicular to the radar beam in order to be visible to the radar, and the locus of points providing field-normal geometry for a given radar location is called the monostatic reflection surface. There is a different such surface (which can be determined by geometry) for each different radar location.

Of more practical importance is the case in which the RF illumination is not normal to the cylinder axis. In that case, the scattered RF energy can intersect the earth at a location different than that of the transmitter, as is shown in Figure 1-2 for energy scattering from a field-aligned irregularity centered in the heater beam at the heater reflection height. The scattering cone always contains the extension past the scatterer of the illuminating ray, and has a common axis of symmetry with the scatterer. For example, when the location of the transmitting site is held fixed, there is again a locus of points where the angle of incidence from the transmitter and angle of scattering to a locus of receiver sites are equal with respect to the geomagnetic field. In that case, the locus of points form what is called the bistatic specular surface. In general, there is a different such surface for each possible pair of transmitter and receiver locations.

If, in the bistatic example shown in Figure 1-2, the heater reflection height is well matched to the bistatic specular surface, the maximum magnitude

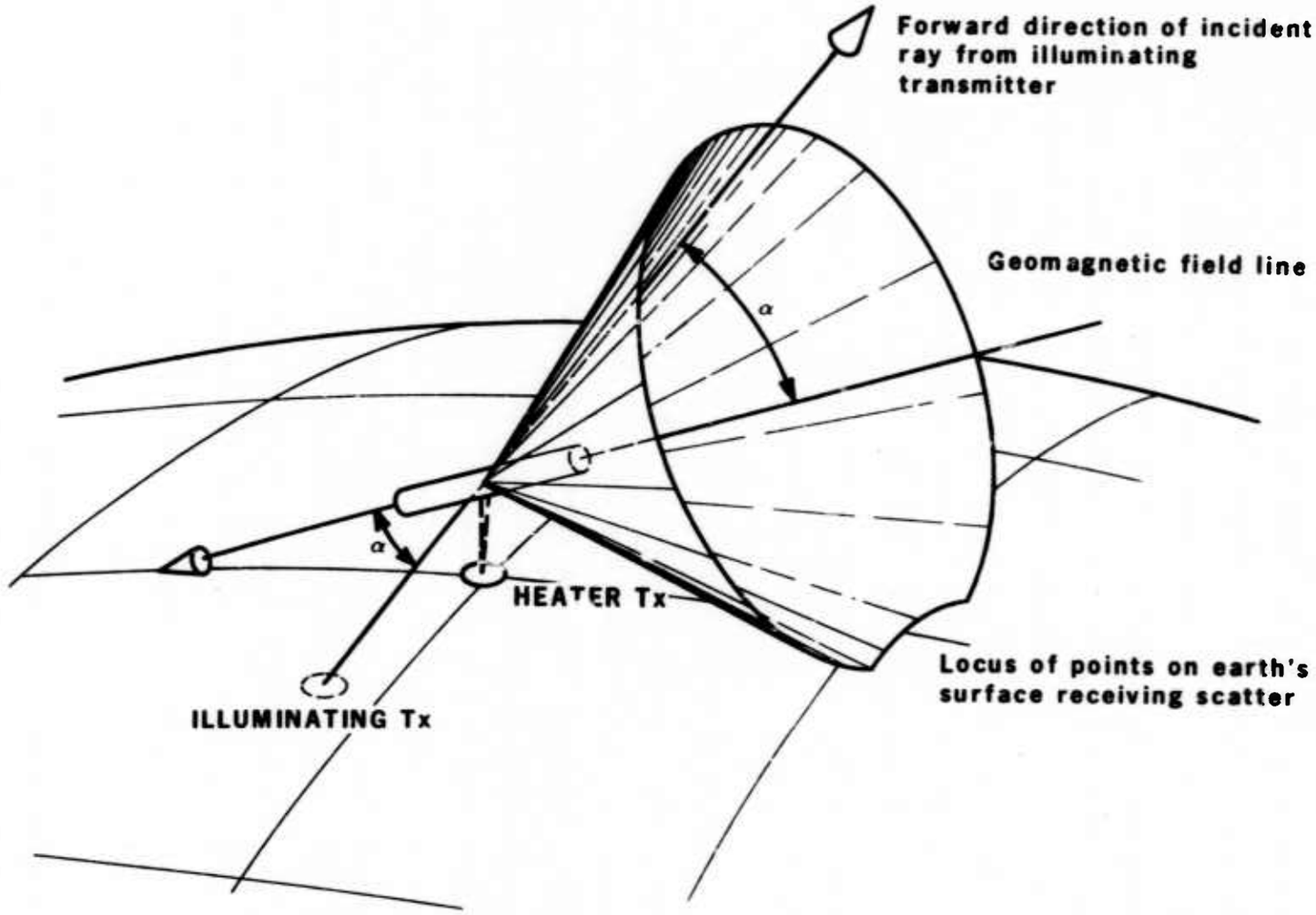

Figure 1-2. Perspective View of a Scattering Cone.

of scattered RF energy reaches the receiving site. For this reason, the heater operating frequency is generally adjusted to provide the best possible match between the heater reflection height and the specular surface for the transmitter and receiver locations of interest. The resulting height is called the specular height.

The relationship between the specular height and the resulting aspect angles (as measured from the axis of the field-aligned scatterer) has been found to be quite critical and plays a major role in the site selection process for transmitter, receiver, and heater. This is because if the aspect angle of the incidence RF energy is 90-n degrees, the best matching specular surface intersecting the earth's surface will have an aspect angle of 90+n degrees. Optimizing transmitter, receiver, and heater locations in order to obtain a specular height that can be maintained for a significant part of a 24-hour period becomes a non-trivial problem. However, when it can be achieved, over-the-horizon communication via VHF is possible.

Section 2

IONOSPHERIC HEATING

Communication by field-aligned scatter from a man-made ionospheric disturbance implies a properly-located, high-power ionospheric heating facility. The ITS Platteville transmitter installation near Denver Colorado, represents a model facility for the purposes of describing heater requirements and heating effects. The following section briefly describes the Platteville heater, the characteristics of the ionospheric disturbance created by the heater, and a summation of general heater requirements.

2.1 PLATTEVILLE IONOSPHERIC HEATING FACILITY

The Platteville transmitter building and two crossed-dipole antenna arrays are shown in plan view in Figure 2-1. The transmitted signal is derived from a single frequency synthesizer the output of which is divided into ten equiphase signals for driving ten separate power amplifiers, each yielding approximately 160 kW output power.

Each power amplifier is connected to a separate element of a broadside (upward-directed) phased array, so the relative phase of the signals from each transmitter must be controlled. Although the feedlines between each power amplifier and its associated antenna assembly are of different length, equi-length lines between a probe near each antenna and a phase comparator located in the transmitter building are used to obtain proper phasing of the ten transmitters.

The ring array antenna system was designed to radiate vertically over the octave bandwidth 5 to 10 MHz with a circularly-symmetrical half-power beamwidth of 20 degrees at midband. The system, designed for right- or

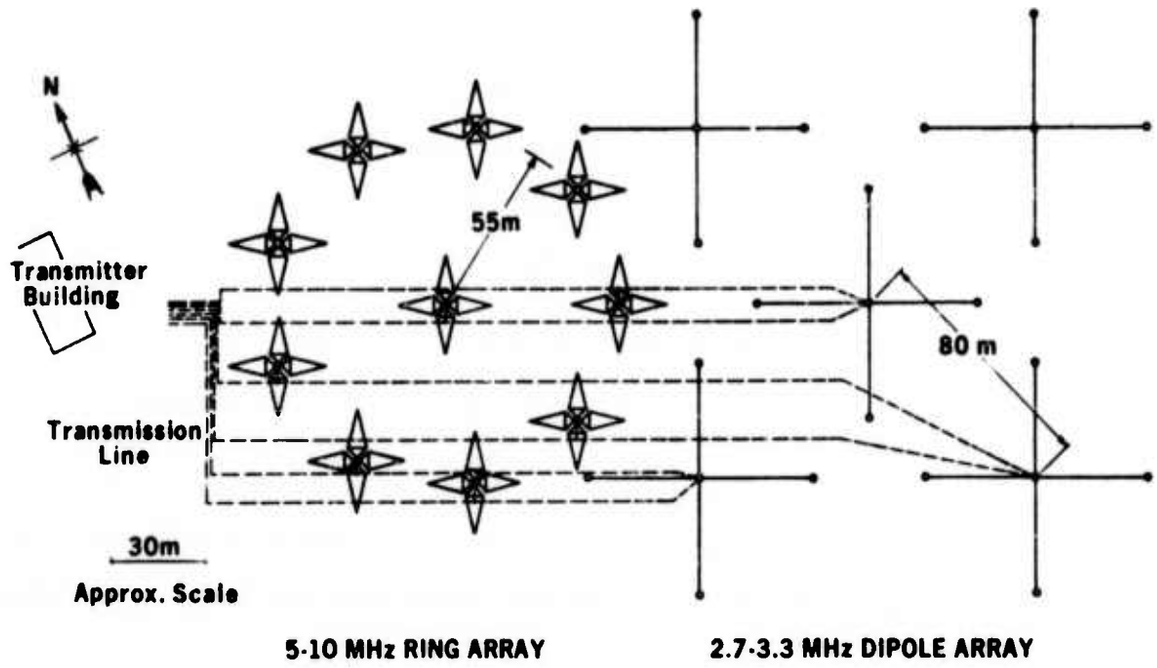

Figure 2-1. Plan View of Platteville Heater Facility.

left-hand polarization capability with a maximum axial ratio of 2 to 1, consists of nine crossed dipole elements on a 110-meter diameter circle, with a tenth crossed dipole in the center. Each element (see Figure 2-2) is made from crossed pairs of 30-meter conical monopoles 10 meters above a galvanized steel mesh ground screen.

The second crossed dipole array was constructed to permit operation during nighttime in the vicinity of 3 MHz with characteristics similar to the ring array. As shown in Figure 2-1, this second array consists of four crossed dipoles equispaced on a circle almost 160 m in diameter with a fifth pair of elements in the center. A separate transmitter drives each dipole element in a frequency range of 2.7 to 3.3 MHz. Each 5-wire dipole is suspended 25 meters above a steel mesh ground screen.

In addition to the main transmitter facility at Platteville, a vertical incidence ionosonde, located at Erie, Colorado, approximately 26 km west of Platteville, is used to estimate the virtual height of the electron plasma frequencies within the heater's operating frequency range. The altitude of the resulting heater disturbance is estimated from the virtual height at the heater operating frequency using a real-time true height profile computer processing algorithm developed at ITS.

2.2 IONOSPHERIC DISTURBANCE CHARACTERISTICS

The principal effect of the ionospheric heating facility is the creation of a disturbed volume of measurable radar cross section. The cross section varies with time of day, ionospheric electron density profile, ionospheric stability, heater power and heater frequency. Measurements of apparent cross section of the disturbance have been made under various heater operating conditions. A detailed discussion of many of these measurements may be found in References 2 through 9. The following discussion emphasizes the observations made on bistatic communication links operated by Barry Research.

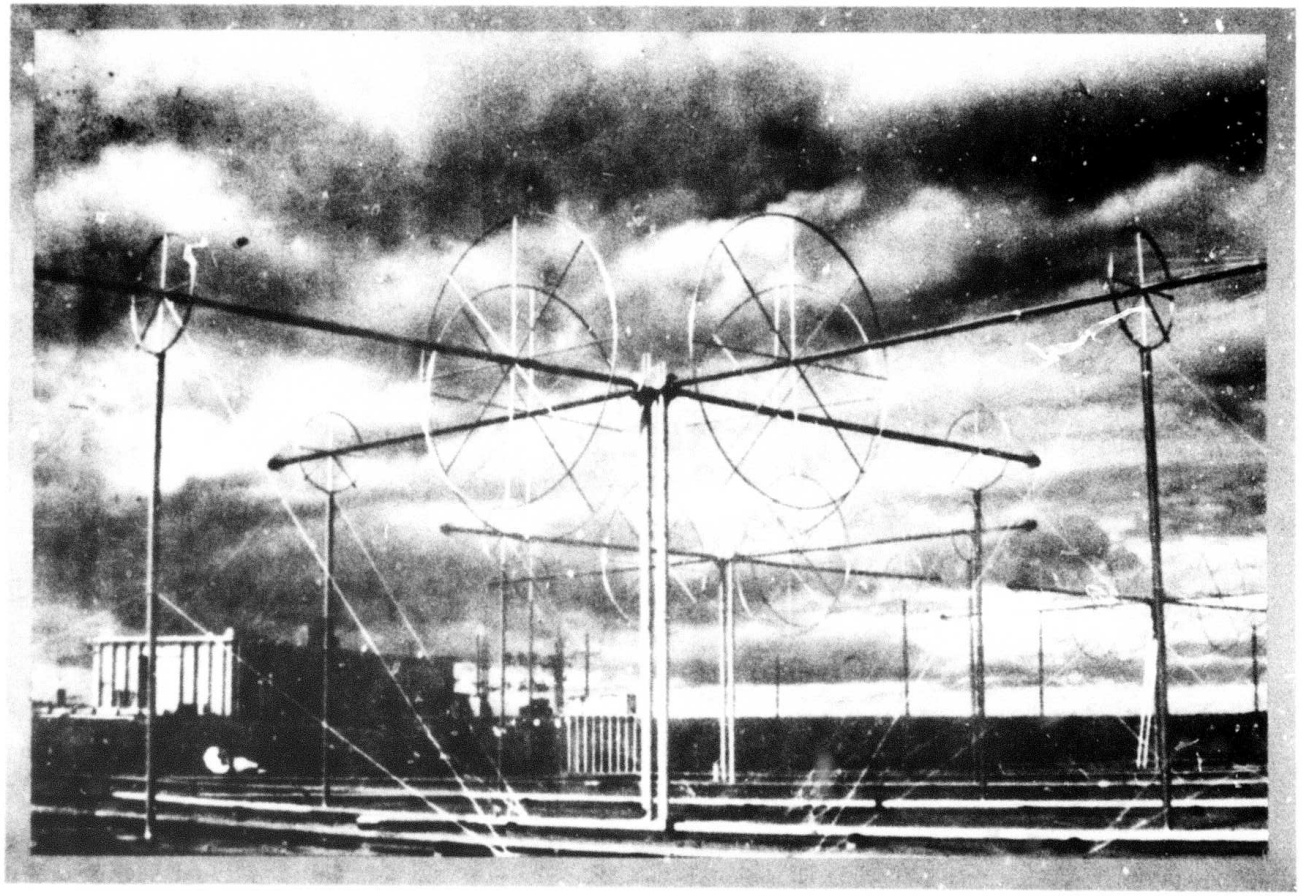

Figure 2-2. Element of 5-10 MHz Ring Array at Platteville Heater Facility.

2.2.1 Variation of Scatterer Cross Section

Figure 2-3 shows highest observed radar cross sections observed as a function of signal frequency. The data includes all times of day and was collected on bistatic paths with a subtended scattering angle of 70-90 degrees. Each cross section value is a median, obtained from a set of 20 samples of received signal power in a 2-second period.

Figure 2-4 indicates the variation of observed median radar cross section (using the same 2-second sampling technique) for the bistatic paths vs hour of day during the months of September to November. The curves labeled (1) represent observations for paths selected for optimized daytime signal scatter, while the curves labeled (2) were observed on a path yielding a bistatic specular height better suited for the higher altitude of the nighttime heated volume. Solid lines show peak values; dashed lines indicate mean values; circled dots identify median values if they are greater than 3 dB below the mean. Note that while peak values vary between approximately 30 and 70 dBsm, median values remain between 30 and 50 dBsm. Note also the dips in observed cross section circa 0800 and 1600 heater local time. The first dip is attributed to the difficulty of the heater to provide a disturbance at the appropriate specular height during the rapidly changing ionization conditions shortly after dawn. The second dip, which occurs during stable early afternoon conditions, has not been satisfactorily explained.

2.2.2 Effect of Heater Power on Observed Cross Section

Considerable effort was expended to determine the effect of the heater transmitter power on the observed cross section. Figure 2-5 presents a summary of some of the observed data at various times of day. The variability of the data may result in part from the difficulty in establishing the effective radiated power (ERP) of the heater. Maximum ERP of the Platteville heater,

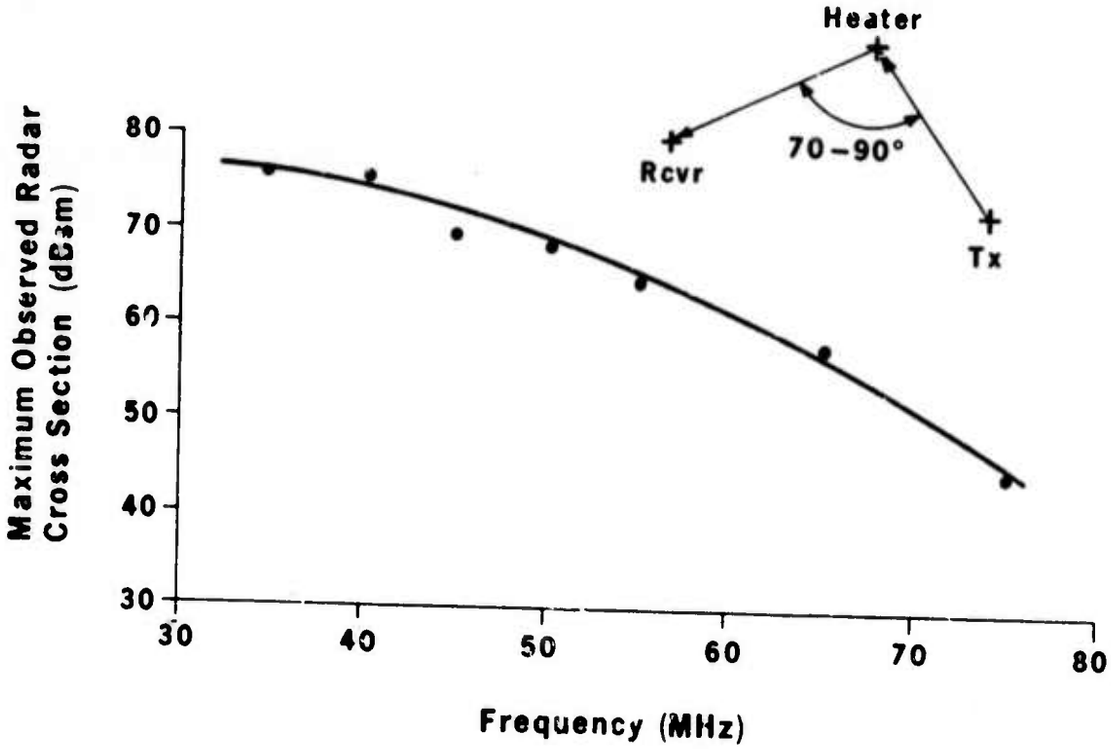

Figure 2-3. Peak Observed Radar Cross Section of Disturbance Volume on Bistatic Paths vs Frequency.

used to obtain the data in Figure 2-5, has been estimated to result from a 62 dBW (1.6 MW) transmitter output amplified by an 18 dBi maximum antenna gain.

The data implies an approximately linear relationship between radar cross section and heater power in the daytime and a less strong dependence at night.

2.2.3 Cross Section Decay After Heater Turnoff

Figure 2-6 shows the relative observed cloud cross section vs time after termination of heater power for both daytime and nighttime. The observed effect is a function of the time of day and the observing radar frequency with faster decay observed during daytime and as radio frequency increases.

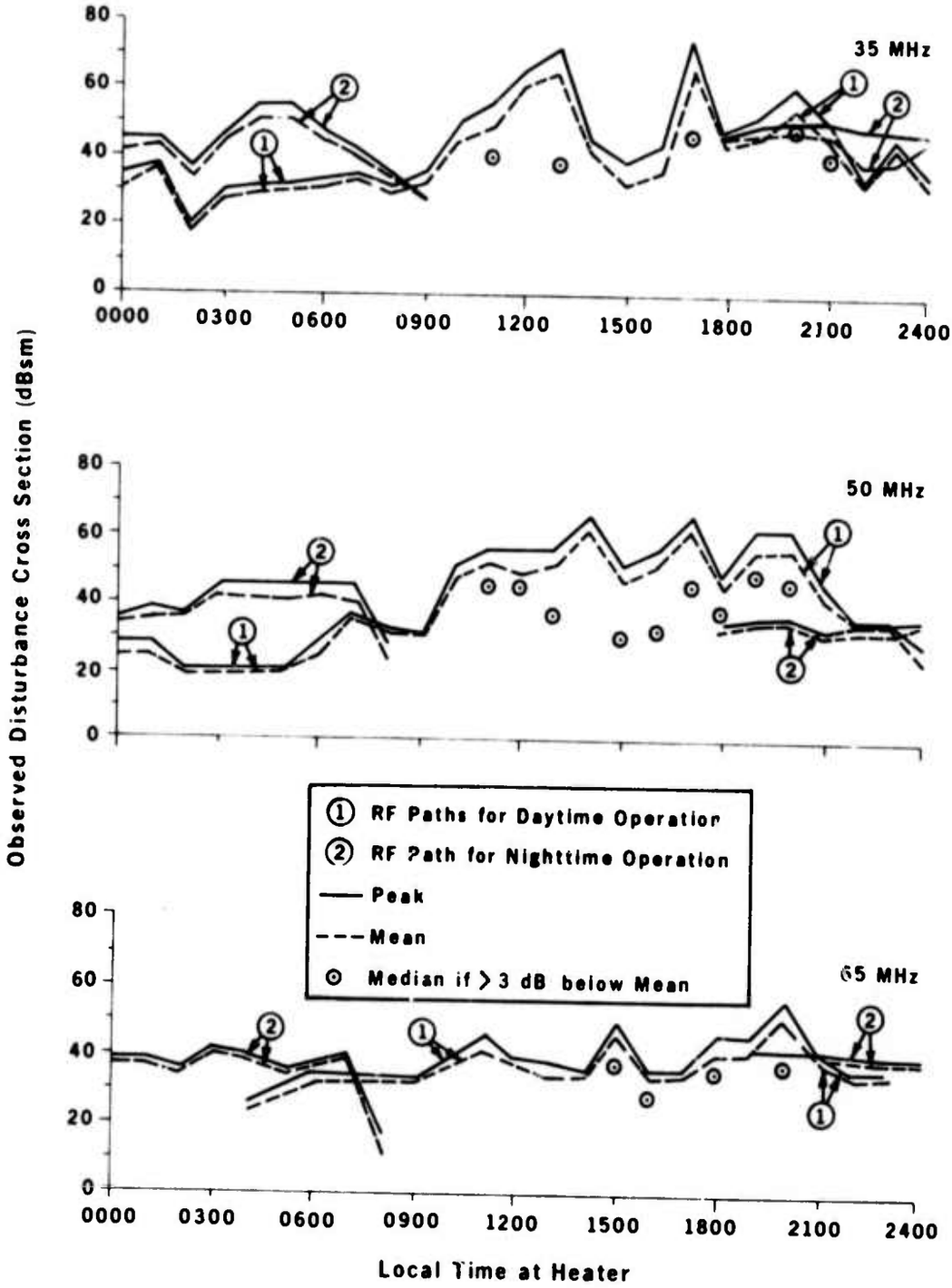

Figure 2-4. Observed Radar Cross Section of Disturbance Volume on Bistatic Paths vs Time of Day During Autumn Months.

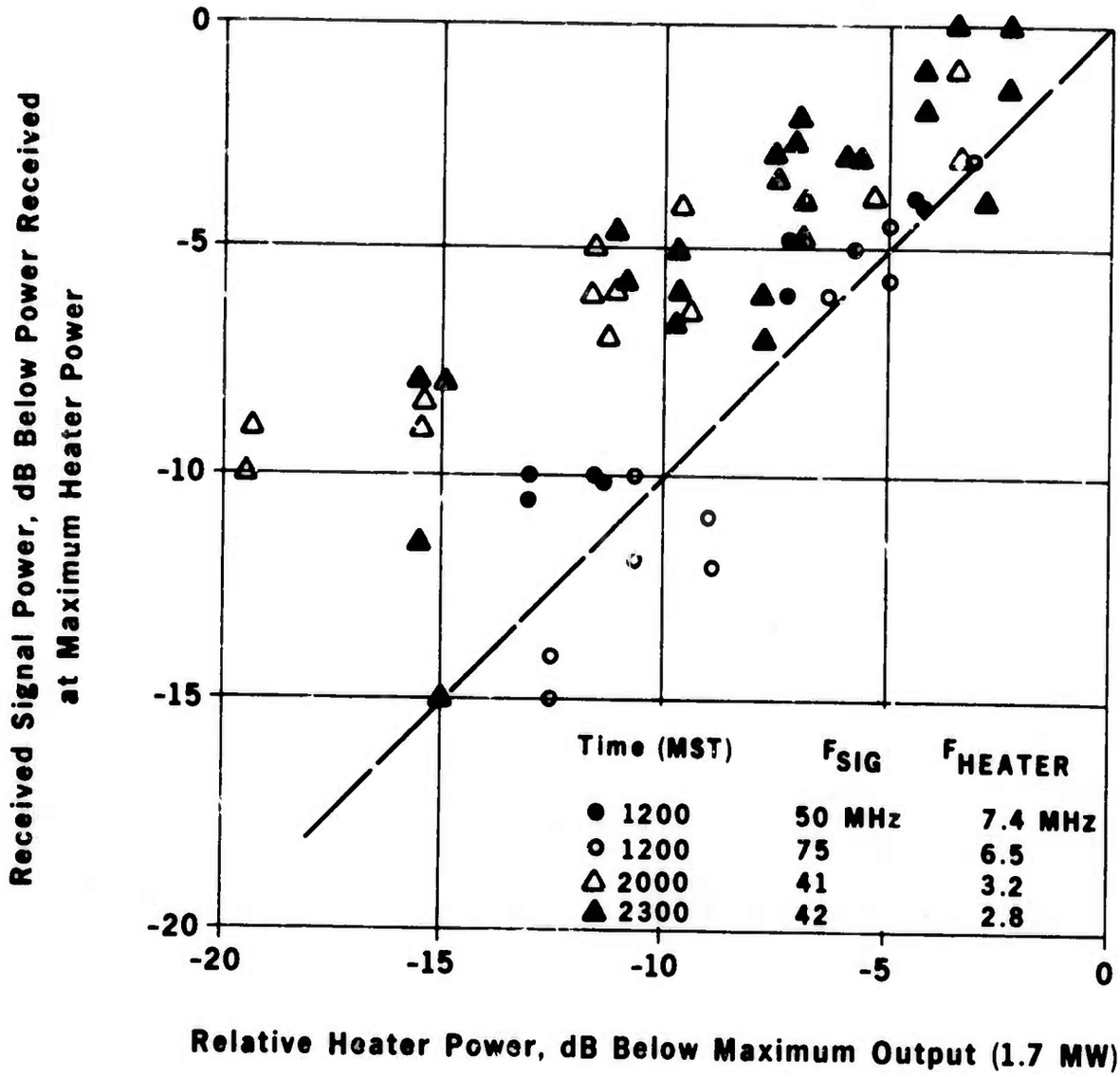

Figure 2-5. Observed Change in Radar Cross Section vs Relative Heater Transmitter Output Power.

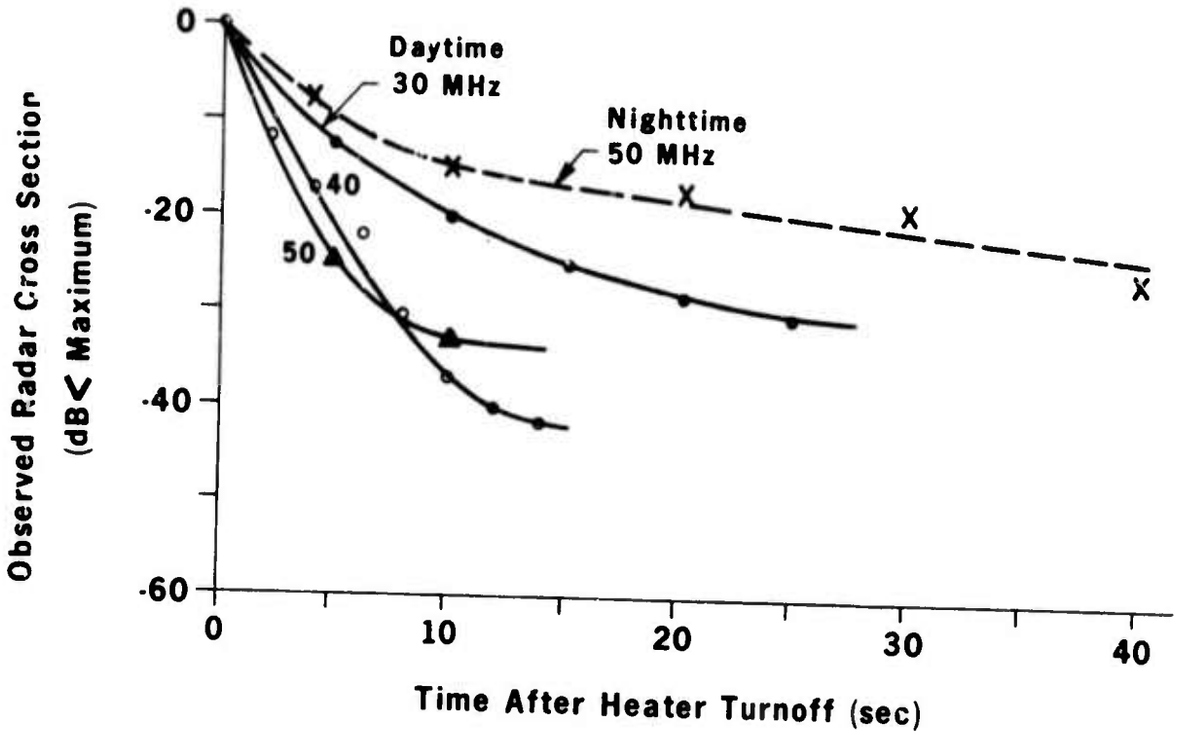

Figure 2-6. Observed Radar Cross Section After Termination of Heater Power.

2.2.4 Effect of Alternate Heater Operating Modes

The above discussion suggests cross section enhancement at lower VHF radar frequencies could be created with less average heater power by pulsing the heater rather than operating CW. Observed data, such as that presented in Figure 2-7, lend credence to the theory. The figure shows observed cross sections at 40 MHz under various conditions of peak power, duty cycles, and time of day for 33 pps heater pulsing.

Other techniques to enhance the observed cross section have been tried without evidence of success. These include the splitting of heater power between two output frequencies to increase the potential disturbance volume. (Figure 2-8 shows the result of one such test indicating no variation in cross section yield beyond the normal uncertainty associated with single frequency

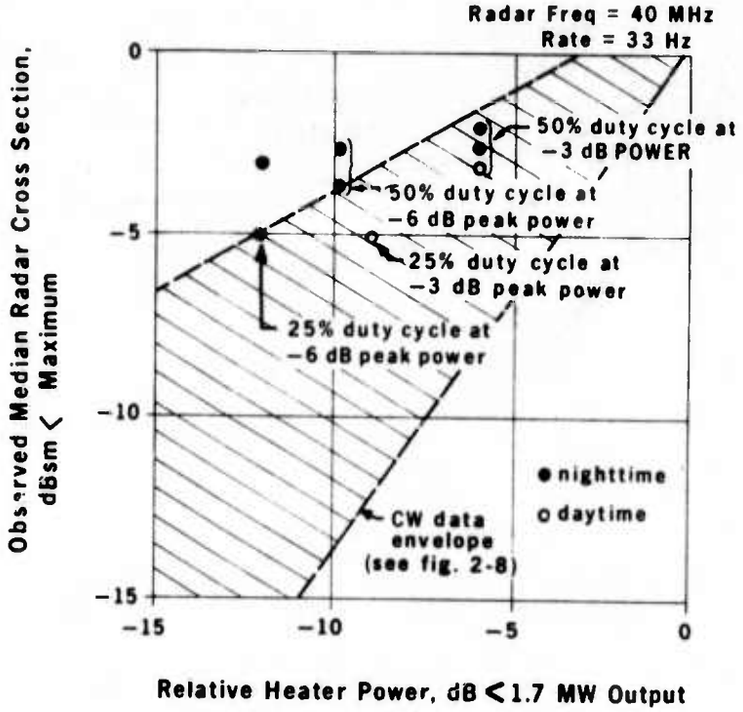

Figure 2-7. Observed Radar Cross Section With Heater Pulsing Relative to Full Power CW Operation.

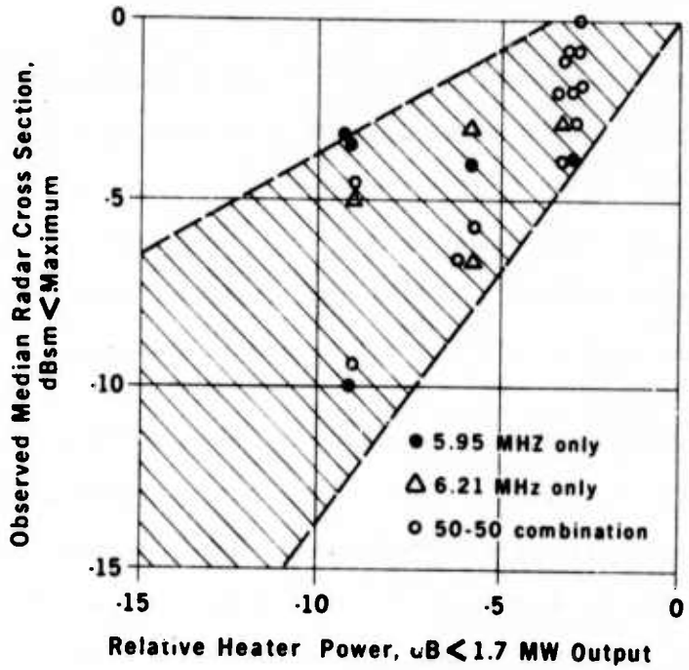

Figure 2-8. Observed Change in Radar Cross Section vs Relative Heater Output Power for Double Resonance Test.

Although diurnal variation of the ionospheric and tropospheric bending of the VHF comm signal from transmitter to cloud and cloud to receiver means the optimum cloud height will vary with time, this variation is of second-order importance. In general, heater frequency management is a problem of attempting to heat at just one altitude for a given communications circuit. Figure 2-10 illustrates that this is no easy task. The figure shows variation with time of day of the estimated plasma frequency at 240 km above Platteville for several days in October 1972. Note the variations from day to day and the rapid changes at sunset. Even more rapid variation occurs at sunrise resulting in the performance decrease evident in Figure 2-4.

Interestingly during nighttime, it was found during Project Steep Cliff that operation at 2.9 MHz seemed to consistently yield the maximum received signal power independent of time of night. Figure 2-11 shows cross section measurements obtained on several nights of testing. This figure should not be construed as implying 2.9 MHz is some nighttime optimum; there were some nights that unacceptable cross sections were obtained on all frequencies in the available range (2.7 - 3.3 MHz). However, experience suggests that once a suitable heater frequency has been found, elaborate frequency management during the night appears unnecessary.

2.3.2 Frequency Management Requirements

Frequency Management of the heater is a vital factor in maximizing scatter cross section for a VHF comm circuit during the daytime hours. Use of a rapid scanning vertical incidence ionosonde near the heater location, in conjunction with a real-time true height computation capability, is mandatory. Such a system was tested during STEEP CLIFF II in which a decision whether or not to change heater frequency was made approximately every half hour. The resulting cross section change observed at 45 MHz on a bistatic path when frequency changes occurred is shown in Figure 2-12. The

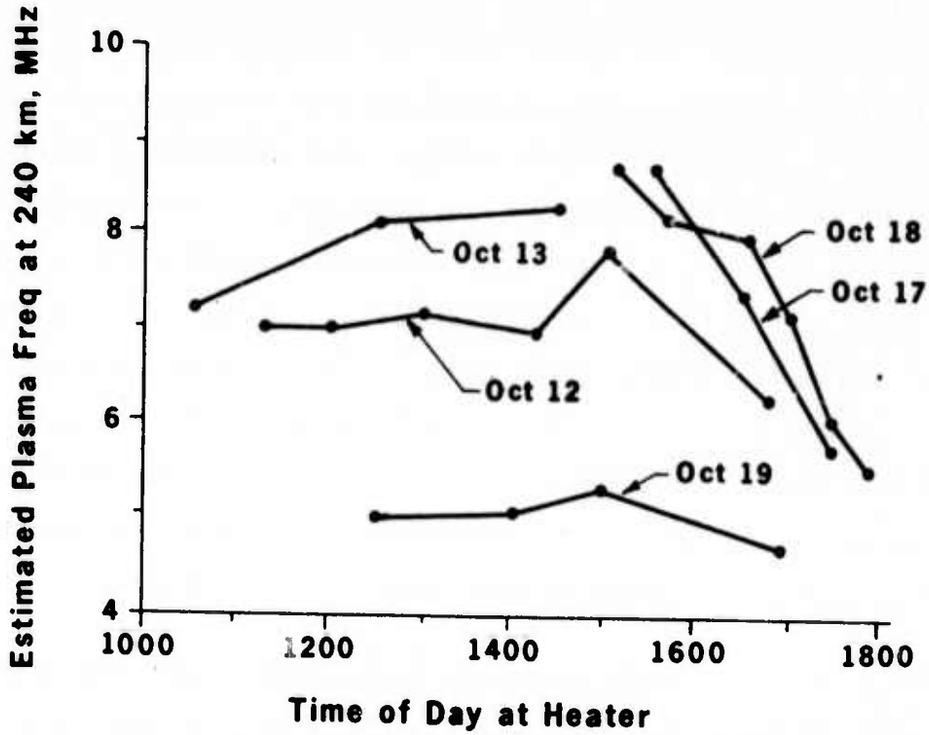

Figure 2-10. Estimated Plasma Frequency Variation at 240 km Over Platteville, Colorado, October 1972.

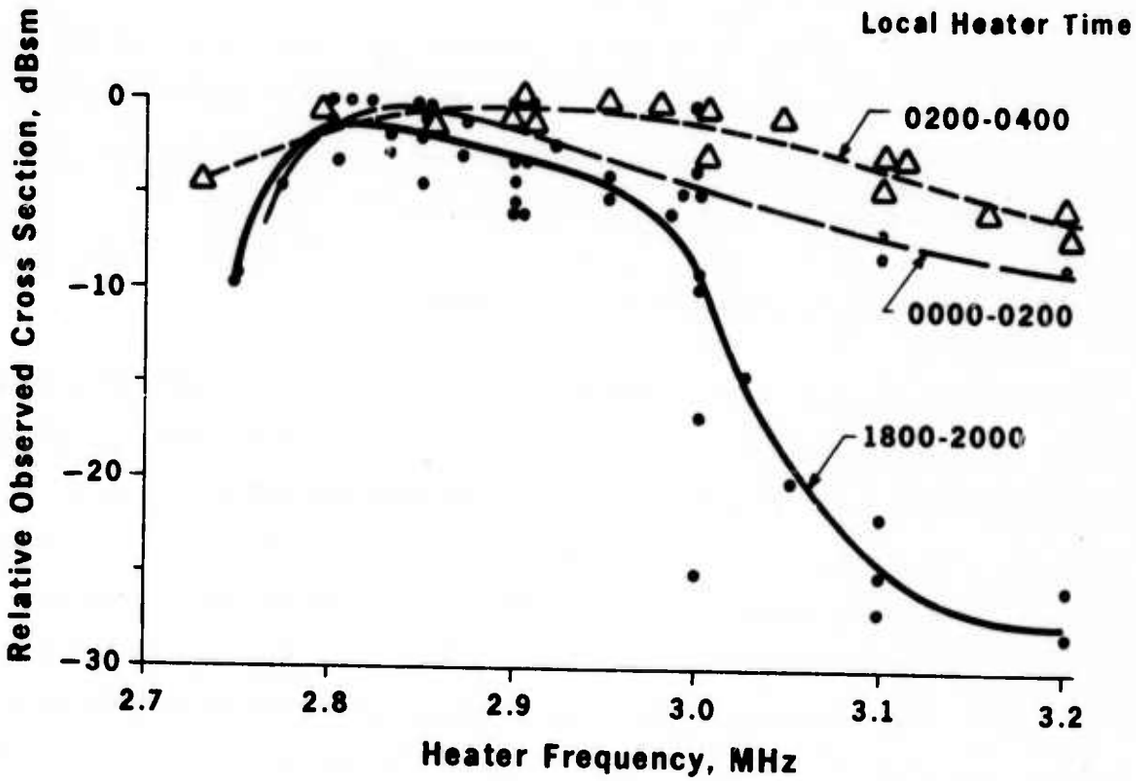

Figure 2-11. Observed Cross Section Variation at Night vs Heater Frequency.

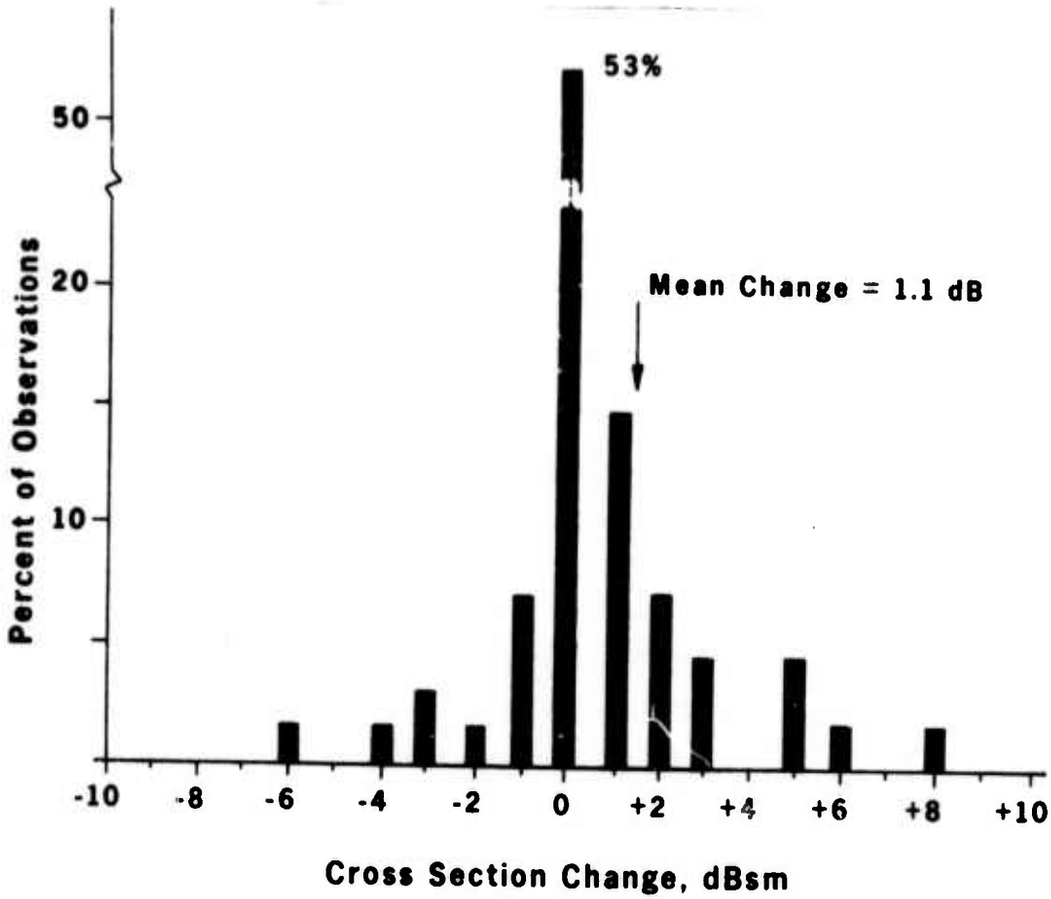

Figure 2-12. Cross Section Change Observed at 45 MHz After Heater Frequency Change During Daytime and Nighttime Operation.

data show that degradation in cross section was observed on 14 percent of the frequency changes, while 33 percent yielded improved cross sections.

Certainly heater frequency management can be performed most confidently when an oblique-incidence ionosonde is used on the communications circuit to measure directly the cross section vs radio frequency as heater frequency is varied. As shown in Figure 2-9, the resulting ionograms indicate received signal power and relative signal time delay spread vs radio frequency, thus giving an overall view of the effect of the cloud on the comm circuit.

2.4 GENERAL SUMMARY OF HEATER REQUIREMENTS

The most reliable communications application involving use of a man-made ionospheric disturbance involves the highly aspect sensitive "field aligned scatter" mode. This mode requires careful consideration of tradeoffs involving desired circuit frequency range, transmitter and receiver site locations, heater location, and desired cloud height. For field-aligned scatter, the heater must be placed closer to the magnetic pole than either the transmitter or receiver site (see Section 4.1).

The numerous field experiments involving the Platteville heater show that it creates a scattering volume which increases in radar cross section as input power increases. Evidence indicates that overall energy savings can be made by pulsing the transmitter. The heater should be capable of operating over at least two octaves (2-8 MHz, for example).

Section 3

VHF SIGNAL CHARACTERISTICS

The following section describes the observed characteristics of VHF signals transmitted over a bistatic path via cloud scatter. The discussion is divided into three significant areas: signal amplitude characteristics, signal power spectrum, and aspect sensitivity as related to direction-finding vulnerability.

3.1 SIGNAL AMPLITUDE CHARACTERISTICS

3.1.1 Signal Fading

The utility of a signal scattered off a man-made ionospheric disturbance is established by the radar cross section of the disturbance volume and the resulting signal fading characteristics.

Figure 3-1 summarizes a series of measurements of deep fading rate. This figure shows day and night measurements of fades per minute 20 dB or more below median observed signal power vs frequency. The measurements show deep fades appear to increase monotonically with frequency and occur at a rate 2-5 times higher at nighttime than during daytime. Long duration fades, common at HF, are very rare on VHF cloud scattered signals.

The effect of increasing fade rate with frequency can be seen in Figure 3-2 which shows examples of facsimile transmission via telephone, via the cloud at 30 MHz, and via the cloud at 50 MHz. The effect of the higher fade rate at 50 MHz, nearly triple the fade rate at 30 MHz, causes the increased incidence of noise, data dropouts, and occasional loss of sync during data transmission.

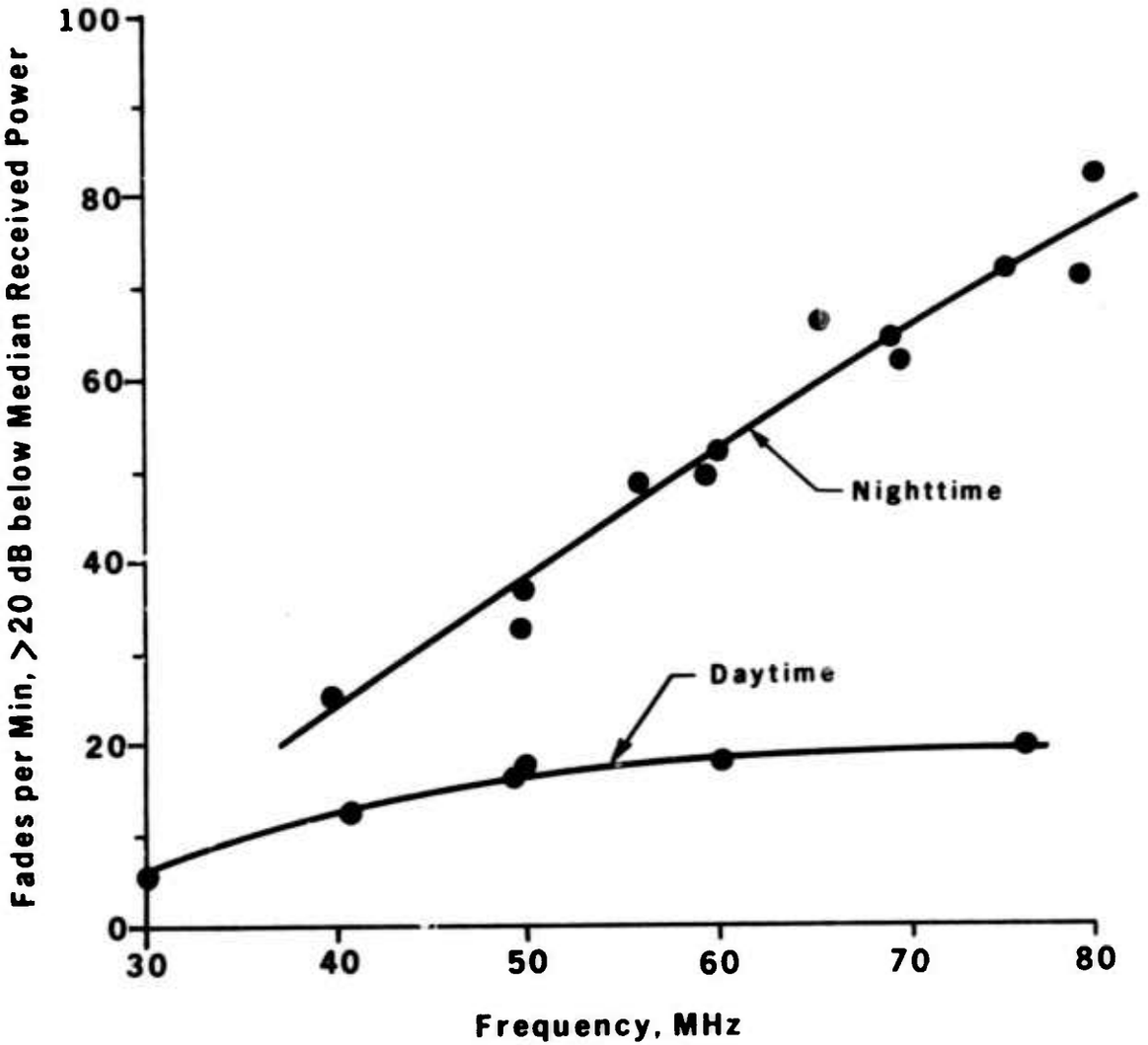

Figure 3-1. Observed Signal Fading on Bistatic Paths.

Via Telephone

Via Cloud-Scatter at 30 MHz

Via Cloud-Scatter at 50 MHz

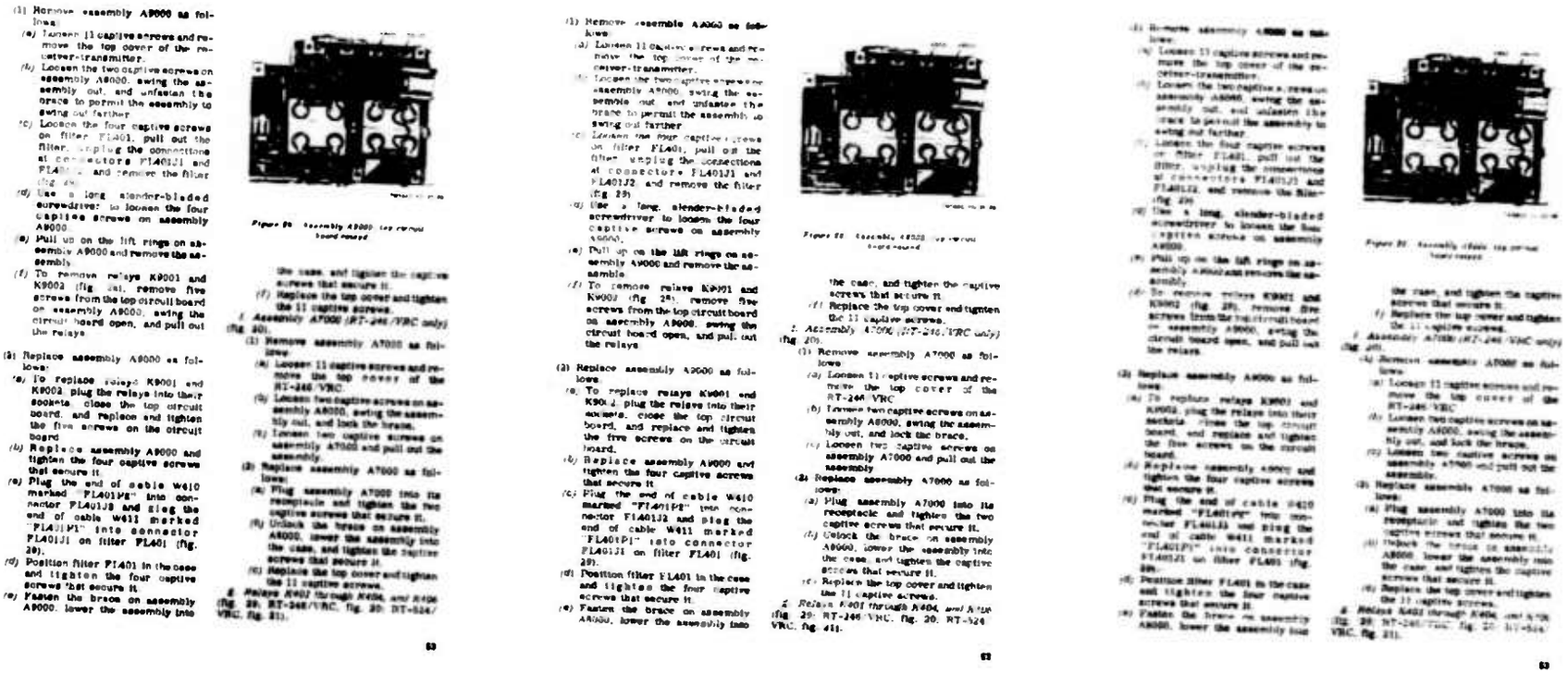

Figure 3-2. Examples of Facsimile Transmission Via Telephone and Cloud Scatter Transmission.

The time distribution of received signal strength resulting from the combination of a large number of waves of random phases and of nearly the same amplitude is Rayleigh-distributed and is represented by the formula:

$$T = e^{-0.693(E/E_m)^2}$$

where T is the fraction of time the instantaneous signal strength exceeds the value E, and E_m is the median value of received signal strength. This distribution is plotted in Figure 3-3 along with daytime and nighttime measurements of signal strength distribution at 40 and 60 MHz. This and other similar data confirms the validity of assuming Rayleigh distribution of signal amplitude independent of time of day or frequency. Similar data at 30 MHz taken a year earlier than the data in Figure 3-3 appears in Reference 9.

3.1.2 Fading Correlation Bandwidth

The correlation of instantaneous signal amplitude of two tones as a function of separation frequency becomes a measure of the degree of distortion to be experienced on amplitude-modulated signals due to selective fading, the maximum usable FM deviation, and the maximum channel data rate. Figure 3-4 shows typical signal amplitude correlation coefficients obtained by measuring instantaneous signal amplitude of two tones separated in frequency by various amounts under different propagation conditions over bistatic paths. The figure shows that the fading correlation bandwidth is less in nighttime than in daytime and shows a diurnal variation by a factor of approximately four.

Another measure of relative fading correlation bandwidth is the time delay spread observed on the cloud-scattered signal from oblique incidence ionograms. Figure 3-5 shows a scatter plot of separation frequency

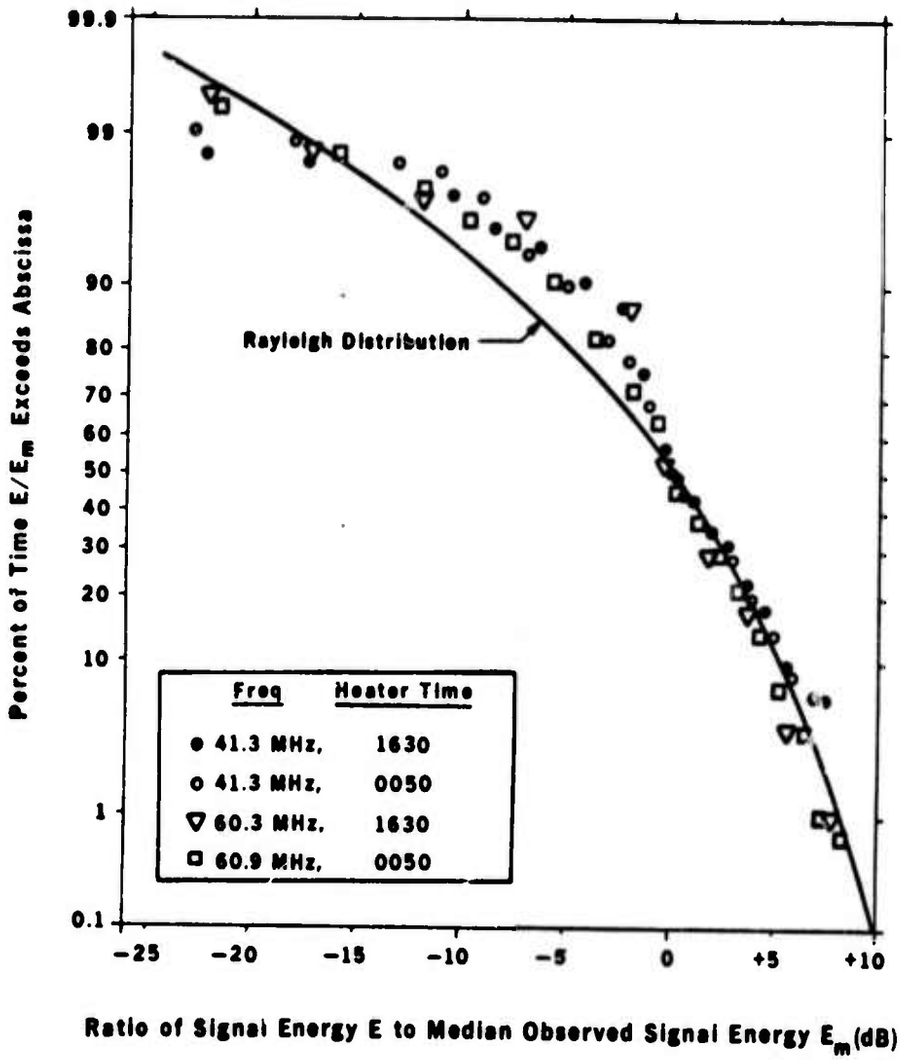

Figure 3-3. Signal Amplitude Distribution.

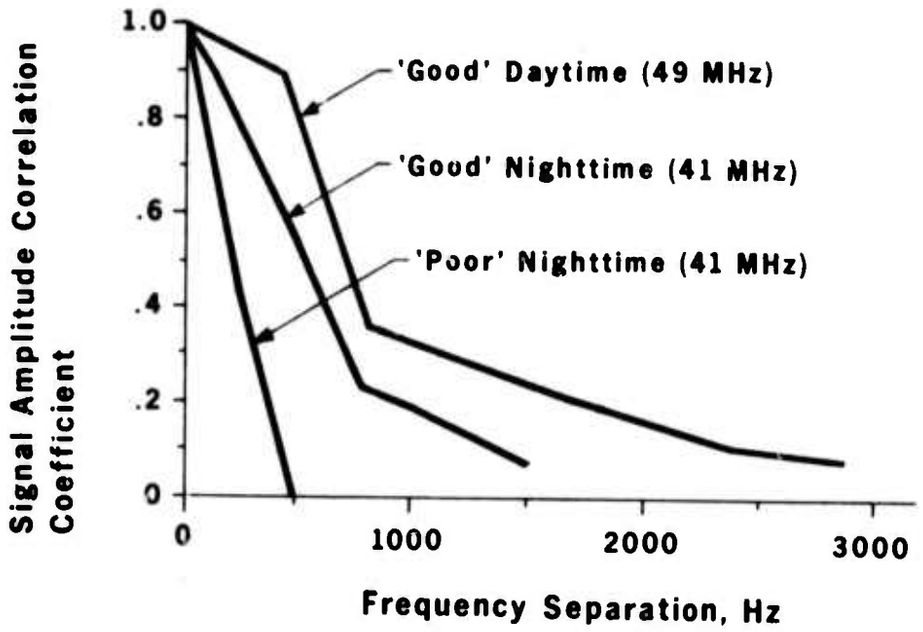

Figure 3-4. Typical Signal Amplitude Correlation Coefficients vs Frequency of Two-Tone Separation.

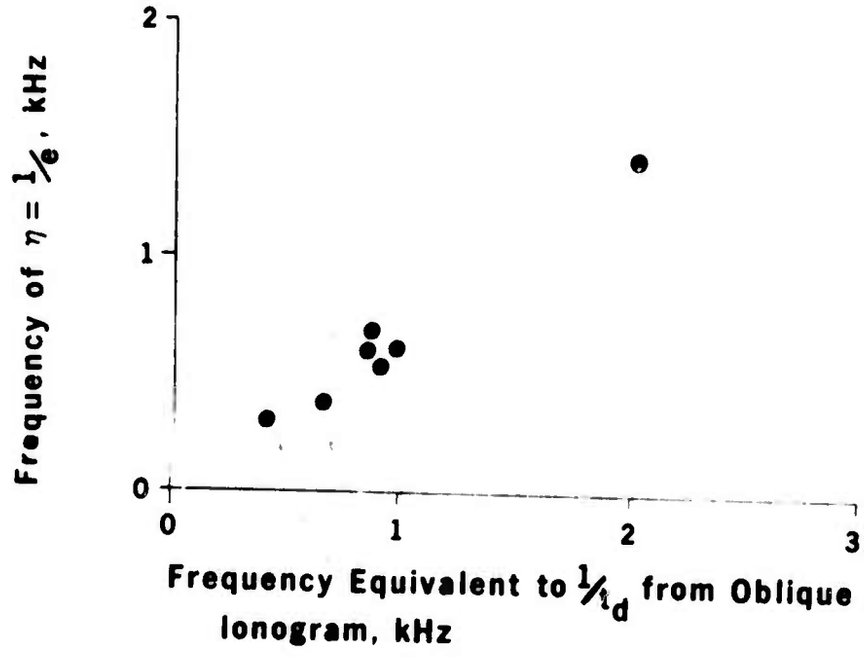

Figure 3-5. Scatter Plot showing Correlation Between Signal Amplitude Correlation Coefficient, η, and Relative Time Delay, t_d, Observed on Ionograms During Fading Measurements.

yielding an amplitude correlation coefficient $\eta = 1/e$ (obtained by interpolating between η values obtained from various amplitude measurement experiments) on the Y-axis and $1/t_d$ (frequency obtained from the reciprocal of the signal time delay, td, observed on an ionogram during each experiment) on the X-axis. The correlation coefficient calculated from these data points is 0.99. Thus, one can use the t_d ionsonde measurements as an indicator of fading correlation bandwidth.

Figure 3-6 shows two ionograms obtained during STEEP CLIFF II showing t_d vs frequency. The time delay spread is related to the range depth of the cloud and shows signal scatter on any frequency to be relatively uniform through the cloud. The striation effect is believed caused by the polarization attenuation characteristics of the horizontally polarized sounder receiver antenna affecting the received power of the signal which is undergoing differing amounts of Faraday rotation vs propagation range (see Reference 6). The significance of this figure to the present discussion is to illustrate the reasonably constant time delay (and hence fading correlation bandwidth) vs frequency of the cloud scattered signal (see also Figure 2-10). This observation is further verified by a summary of t_d data vs frequency for various times of day shown in Figure 3-7.

To obtain a better feel for the variation of fading correlation bandwidth with time of day, Figure 3-8 shows the frequency equivalent to the reciprocal of t_d observed on ionograms at 45 MHz vs local time at the heater. Notice this frequency value increases to a highly variable quantity during daytime (ranging 1.0-2.5 kHz) and falls to 600-1200 Hz at night.

3.2 SIGNAL POWER SPECTRUM

Little data exists on the frequency and time variation of the signal power spectrum. However, the data that does exist, coupled with the characteristics

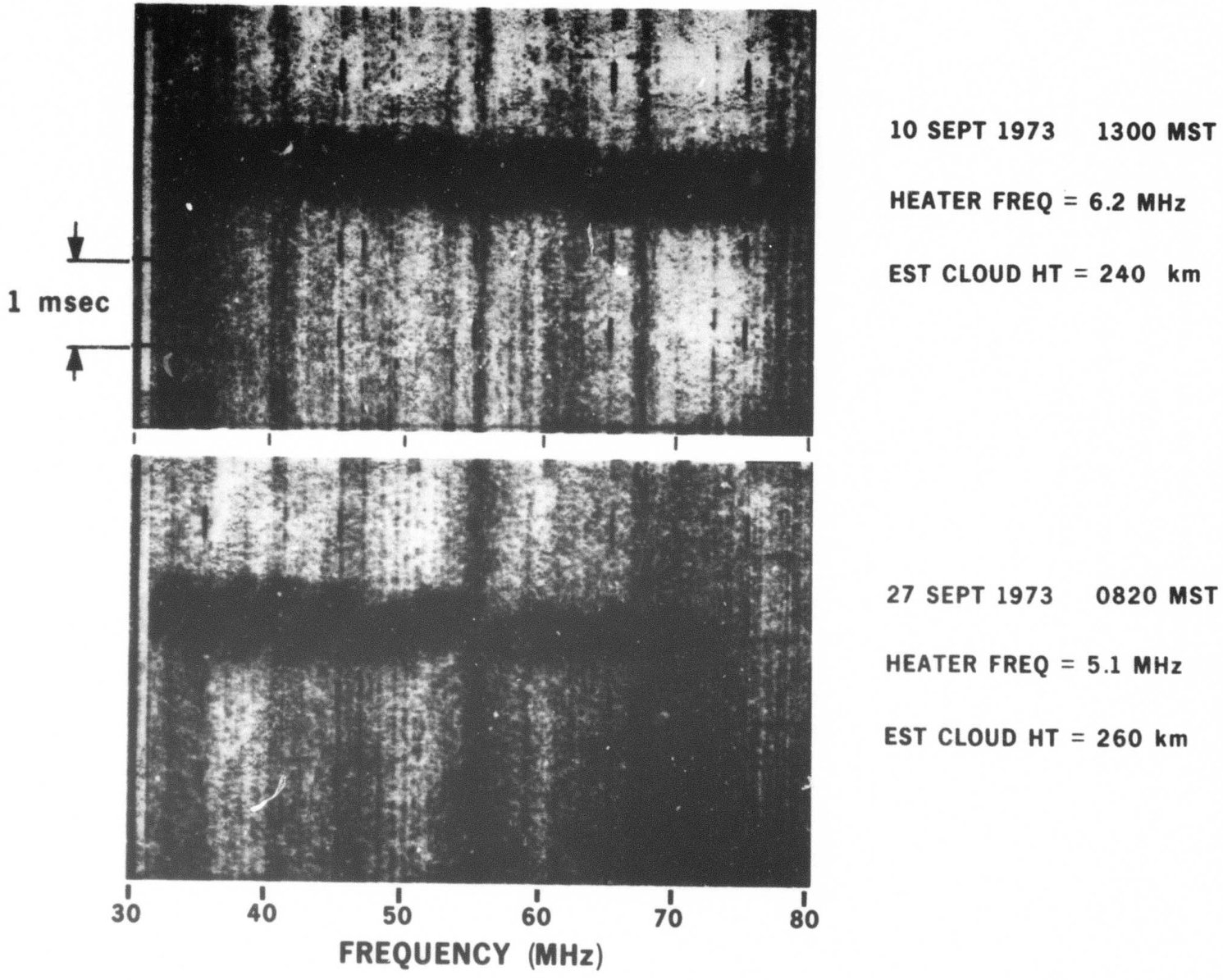

Figure 3-6. Typical Oblique Incidence Ionograms Obtained from Swept Frequency Soundings of Cloud Scattered Propagation.

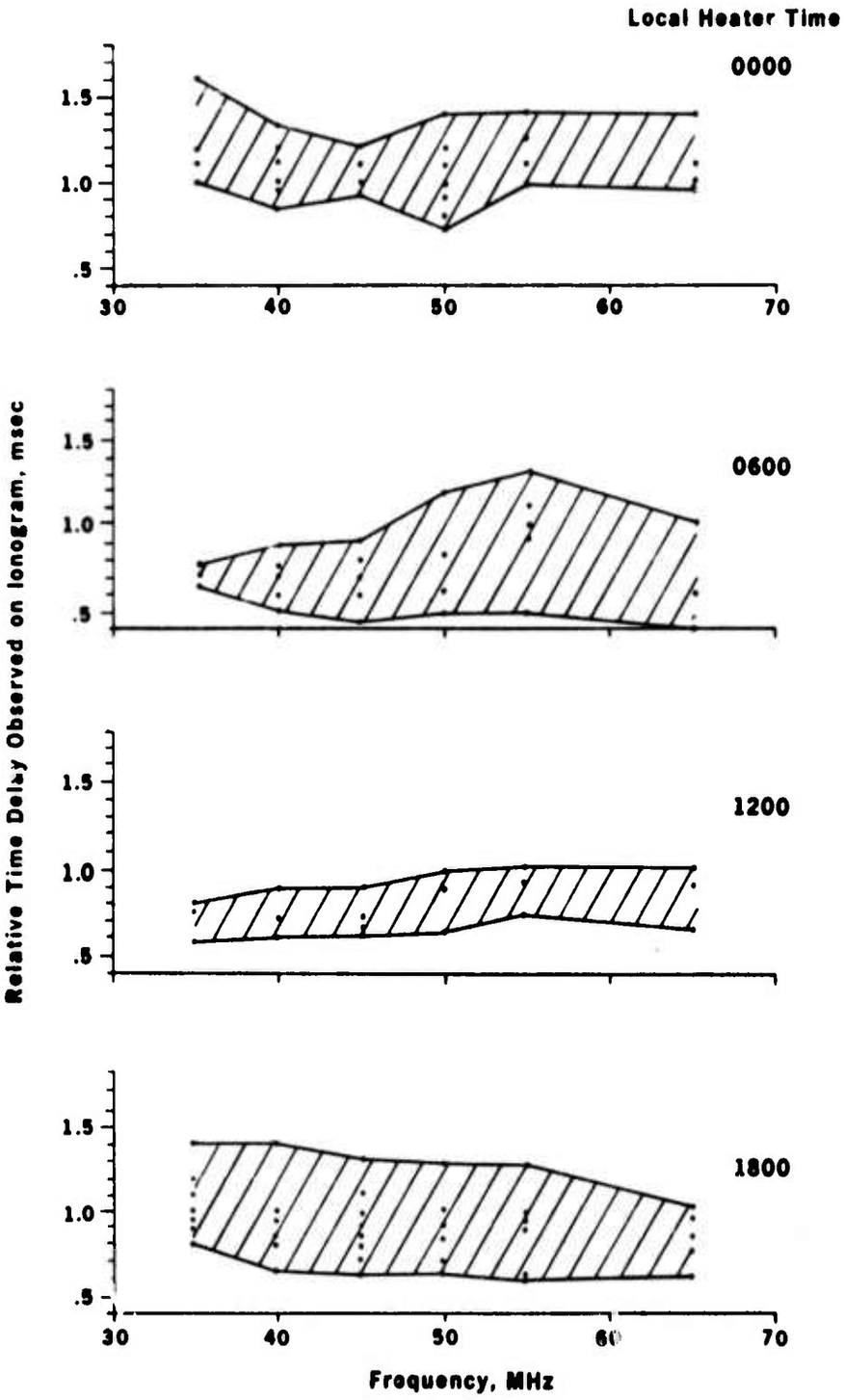

Figure 3-7. Variation of Relative Time Delay Observed on Ionograms vs Frequency.

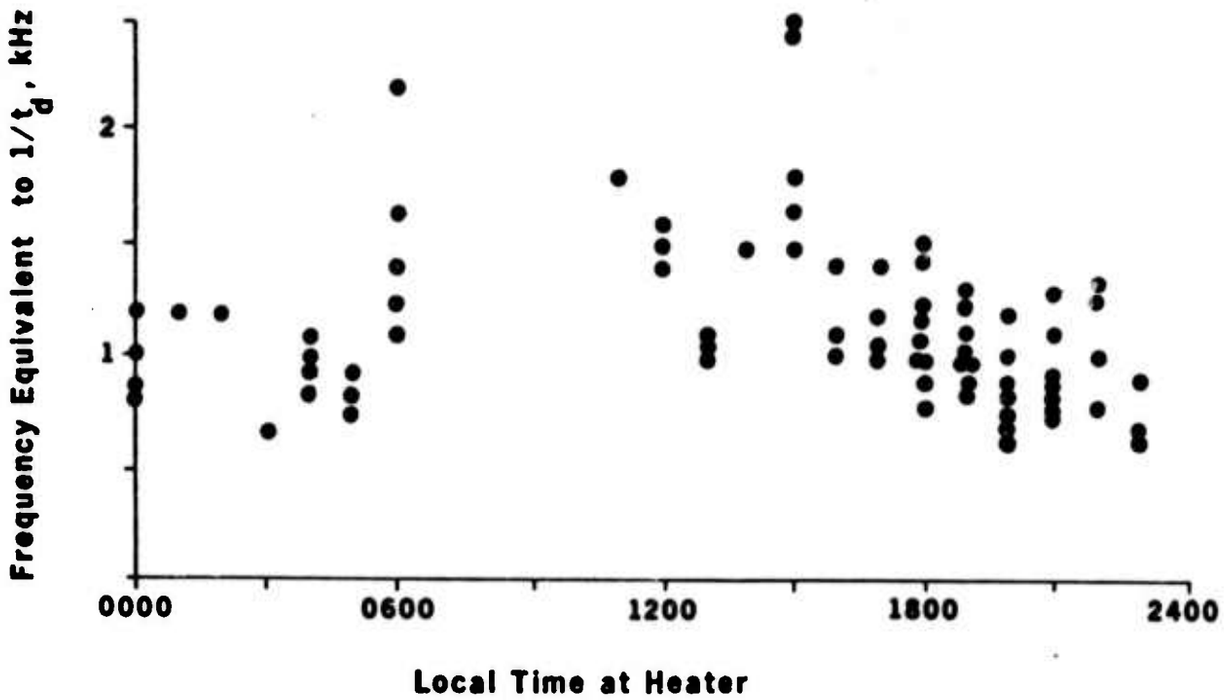

Figure 3-8. Frequency Equivalent to Reciprocal of Total Time Delay Spread on Ionograms vs Time of Day at Heater.

observed from the oblique ionogram data, indicate that, at any given time, there is little variation in the signal power spectrum vs frequency, but that significant diurnal variation occurs. Figure 3-9 shows typical mean signal plus noise power spectra surrounding a CW carrier during daytime and nighttime. The daytime mean spectrum was derived from four spectra samples over a 1-hour period, while the nighttime plot was derived from eight samples. The figure shows spectral spread 20 dB down from the peak level over a 5-Hz bandwidth for the daytime signal and a 16-Hz bandwidth for the nighttime signal. Figure 3-10 shows the distribution of signal power for the two typical spectra and indicates that 90 percent of the signal power is within a 4 Hz bandwidth for the daytime signal and within 10 Hz for the nighttime signal.

The variation in signal power spectra vs time of day is further illustrated during the transition from nighttime to daytime conditions at the heater. Figure 3-11 shows a set of measurements made during STEEP CLIFF II of the signal-plus-noise-to-noise spectrum on 40 MHz during one such transition. Note the narrowing of the spectral spreading as daylight conditions prevail.

Spectrum measurements such as those represented in Figure 3-11, coupled with the greater time delay spread observed on nighttime oblique ionograms suggest a heated scattering region of greater volume during night than day (as would be expected with the higher cloud altitude for a given antenna beamwidth) and with a more rapid relative motion of the irregularities at night. It would appear that the combination of the greater doppler spread of the signal and greater range depth at night produces the increased fading rate observed during these hours.

Figure 3-11 illustrates one other characteristic of the cloud-scattered signal involving doppler shift of the spectrum at 0730. Such doppler shifts are common and can occur at any time. For example, Figure 3-12 shows

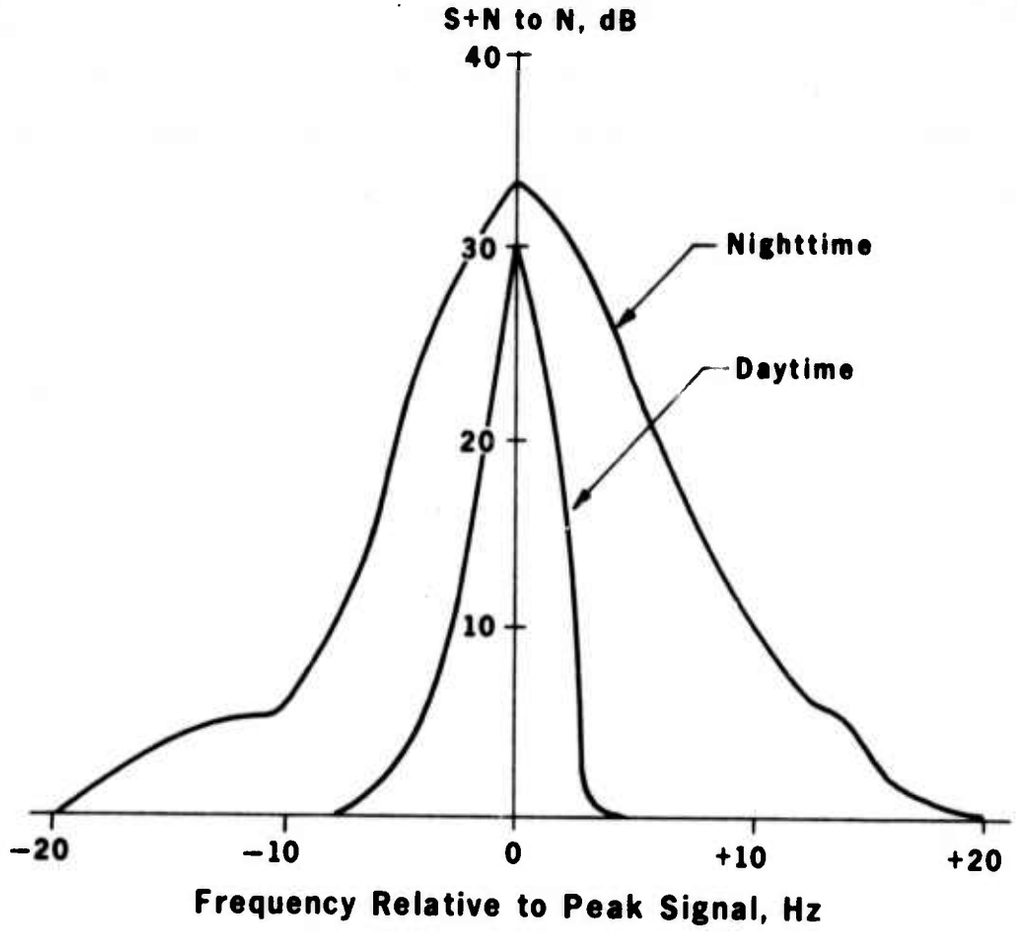

Figure 3-9. Typical Mean Signal Power Spectra for Daytime and Nighttime at 41 MHz.

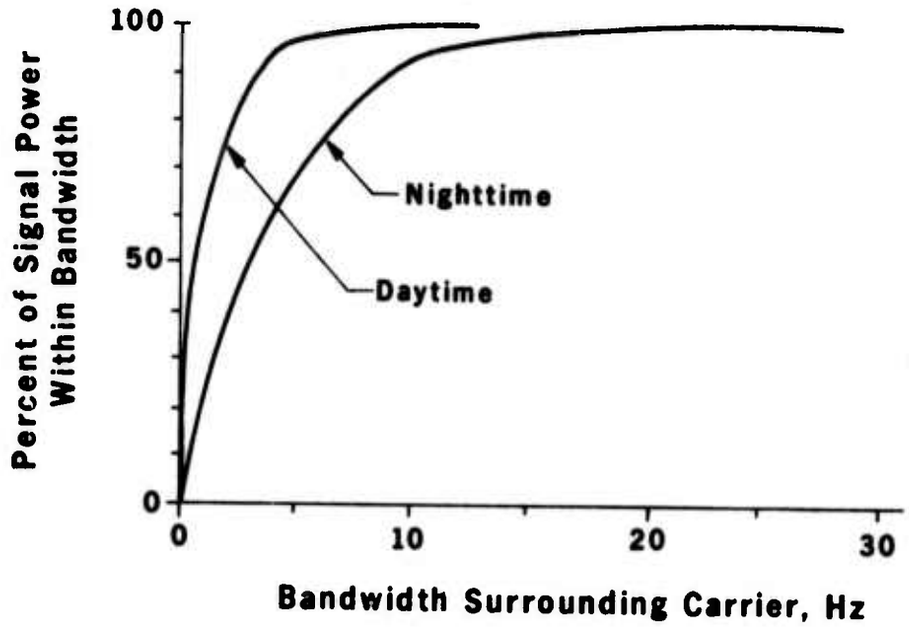

Figure 3-10. Typical Distribution of Signal Power for Daytime and Nighttime CW Signals.

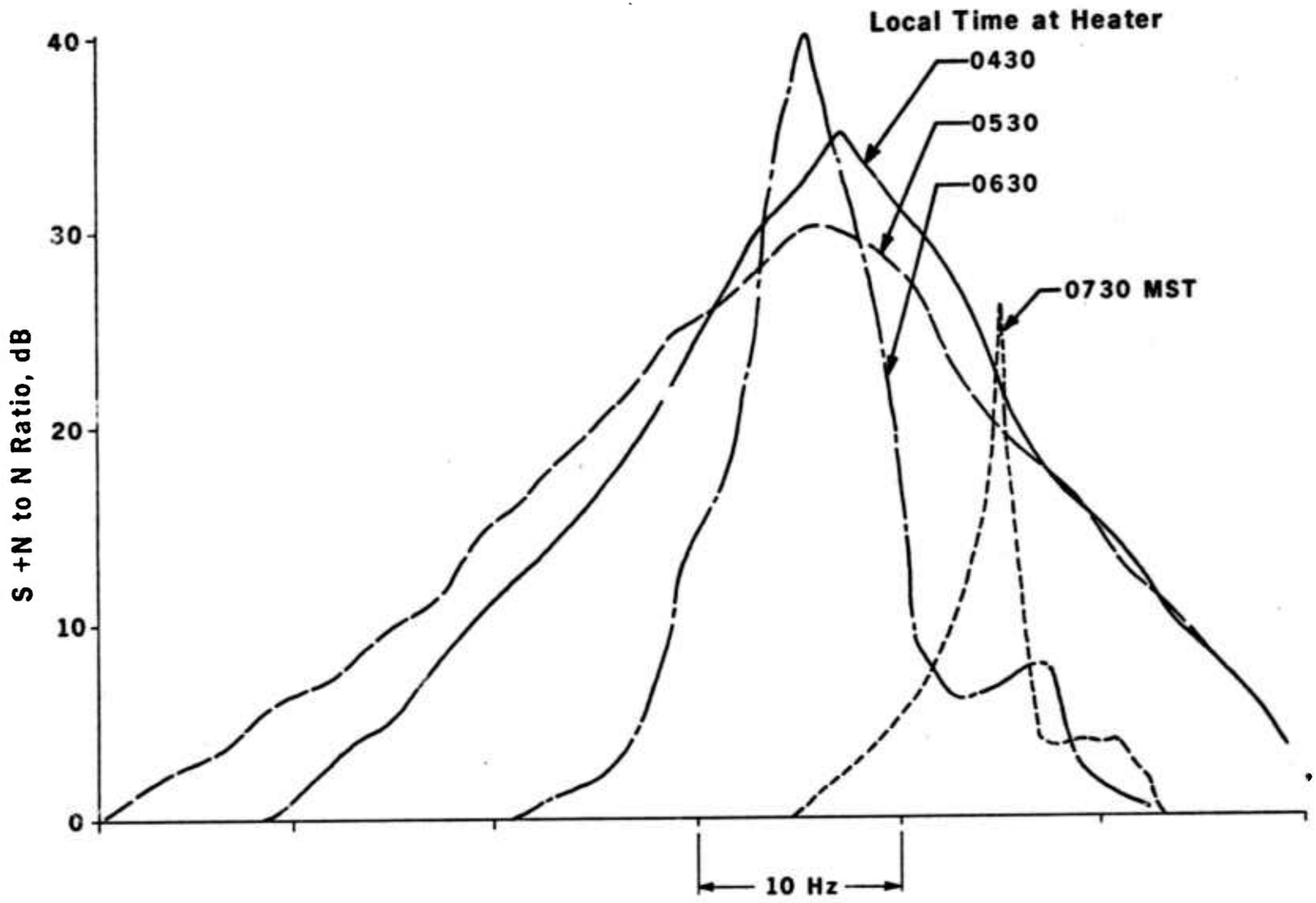

Figure 3-11. Example S+N to N Spectrum Observed During Transition from Nighttime to Daytime.

an example of doppler shift at 41 MHz from +7 Hz to -10 Hz measured on a ≈ 90 deg bistatic path over a 25-minute period. This corresponds to a cloud movement at a rate up to 1.1 km per minute southward and then up to 1.6 km per minute northward winding up at 2247 local time almost 25 km north of its position nearly an hour before. (This motion is confirmed by observation of the signal time delay change on the ionograms recorded during this period). Such cloud movement has been observed in daytime as well (see Ref. 9) and is consistent with the model of a constantly shifting electron density profile of the ionosphere above the fixed-frequency heater causing an upward and northward (or downward and southward) movement of the heated volume.

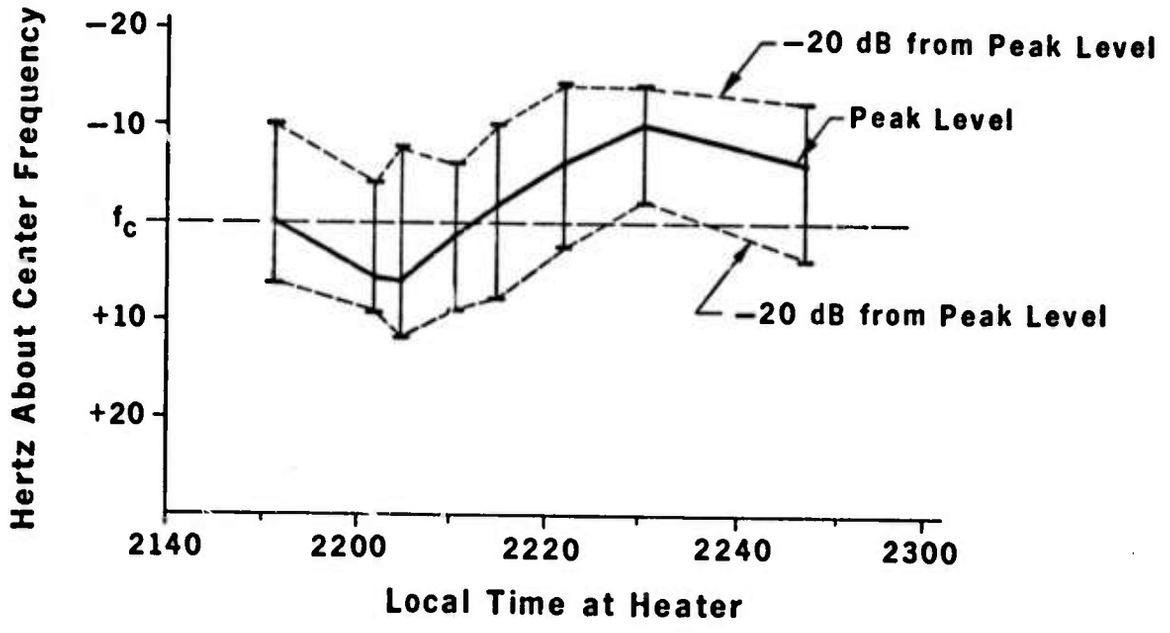

Figure 3-12. Example of Doppler Shift During Nighttime Signal Measurements.

Section 4
COMMUNICATION SYSTEM CHARACTERISTICS

The preceding two sections have summarized the signal transmission characteristics yielded by the man-made ionospheric disturbance. The following discussion presents the major implications of these characteristics on communications circuit design.

4.1 SITE LOCATION REQUIREMENTS

One of the fundamental requirements in utilizing field-aligned cloud scatter for VHF comm is the proper placement of transmitter, receiver, and heater sites. The great aspect sensitivity of the cloud-scattered signal and the necessity that the heater be located closer to the magnetic poles than the transmitter or receiver sites limits the global applicability of the technique. Reference 10 presents specific applications of the technique and indicates site placement requirements. A more general approach to the problem of site locating is discussed in Reference 12.

In general, for a given transmitter location at least two receiver locations will be required for round-the-clock communication, particularly as the communications area departs from the equator. One receiver site will be established for a specular height of cloud associated with daytime operation (e.g., 200-250 km) and the other for a nighttime specular height (e.g., 300-350 km). As illustrated in Figure 2-4, a distinct penalty can occur even at mid-latitudes if the daytime path is used during nighttime.

Other factors will affect site selection as well, particularly those factors involving the heater facility, such as land area for antennas, availability of prime power (or the logistics of providing it), and the effects of RFI

from the heater transmitter operation. In addition, sufficient land area will be needed at the VHF receiver site for spacing of antennas for space diversity signal reception.

4.2 SYSTEM ENERGY REQUIREMENTS

Required system energy for a comm circuit can be defined as:

$$E_j = \frac{P_T G_T G_R}{B} \quad \text{joules} \tag{4-1}$$

where P_T = transmitter power, watts

G_T = transmitter antenna gain in direction of cloud

G_R = receiver antenna gain in direction of cloud

B = received noise bandwidth, Hz

For scatter off a man-made ionospheric disturbance

$$E_j = \left[\frac{S}{N}\right] \left[\frac{64\pi^3 R_1^2 r_2^2 P_N}{\sigma \lambda^2}\right] \tag{4-2}$$

where $\frac{S}{N}$ = received signal-to-noise ratio

R_1 = distance from transmitter to cloud, meters

R_2 = distance from cloud to receiver, meters

P_N = noise power per hertz, watts

σ = apparent cloud cross section, square meters

λ = wave length of signal, meters

Figure 4-1 shows required system energy in dB above 1 joule vs frequency for a cloud-scatter circuit assuming:

$S/N = 10$ dB

$R_1 = R_2 = 1000$ km

$P_N = 10$ dB > kTB = -194 dBW

$\sigma = 40$ dBsm

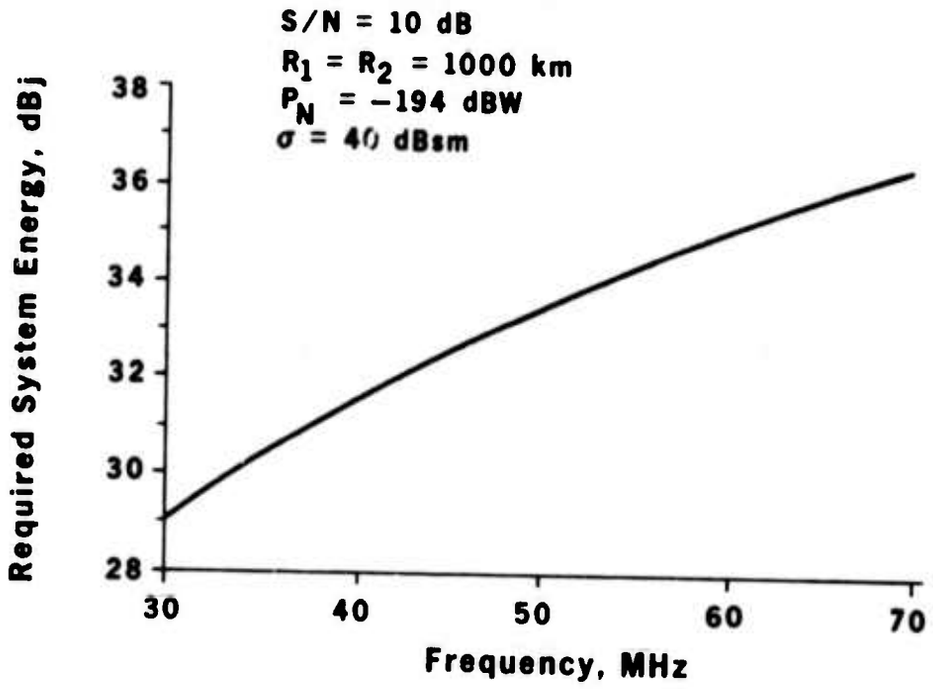

Figure 4-1. Required System Energy vs Frequency for a Cloud-Scatter Circuit.

The curve shows, for example, that at 40 MHz a 3 kHz voice circuit using a 1-kW transmitter would require 36.5 dBi overall antenna gain (equivalent to four 12.5 dBi yagi antennas at both ends of the circuit).

Utilizing Figure 4-1, the lowest median cloud cross section from the data in Figure 2-7, and Rayleigh signal amplitude distribution, one can get some idea of the system energy vs frequency required to ensure various probabilities of attaining an S/N ratio of at least 10 dB. Figure 4-2 shows these E_j values for probabilities of 50, 90, and 99 percent.

4.3 ANTENNA CONSIDERATIONS

Antenna system design at the transmitter and receiver sites is an important factor in maximizing system energy. Figure 4-3 can serve as a guide in

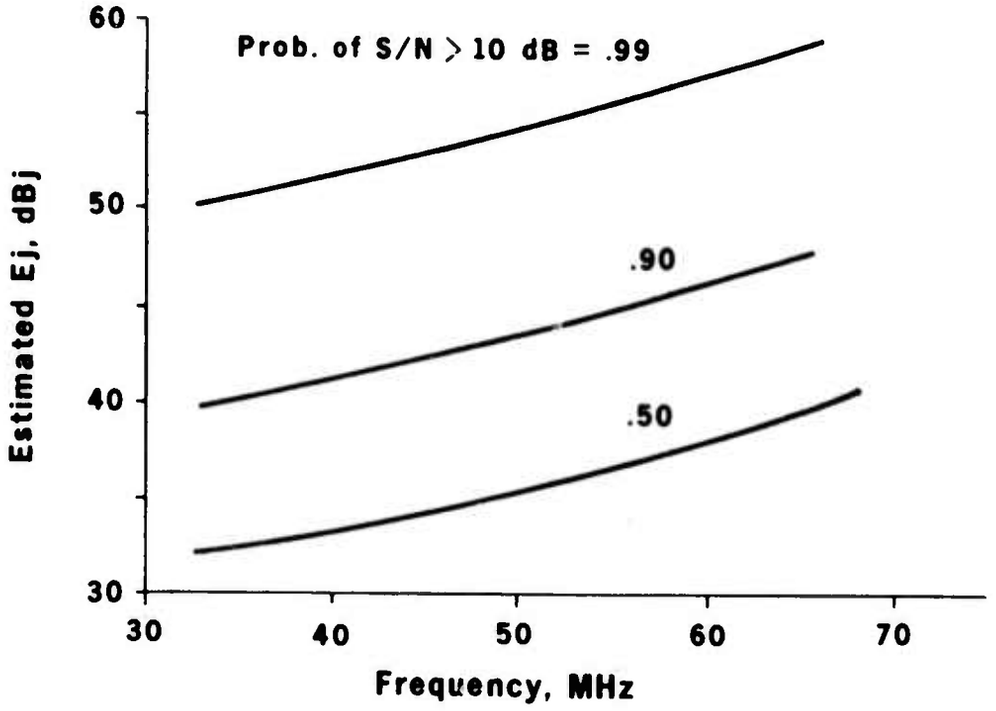

Figure 4-2. Estimated System Energy Required to Ensure S/N > 10 dB vs Frequency for a 3-kHz Cloud Scatter VHF Circuit.

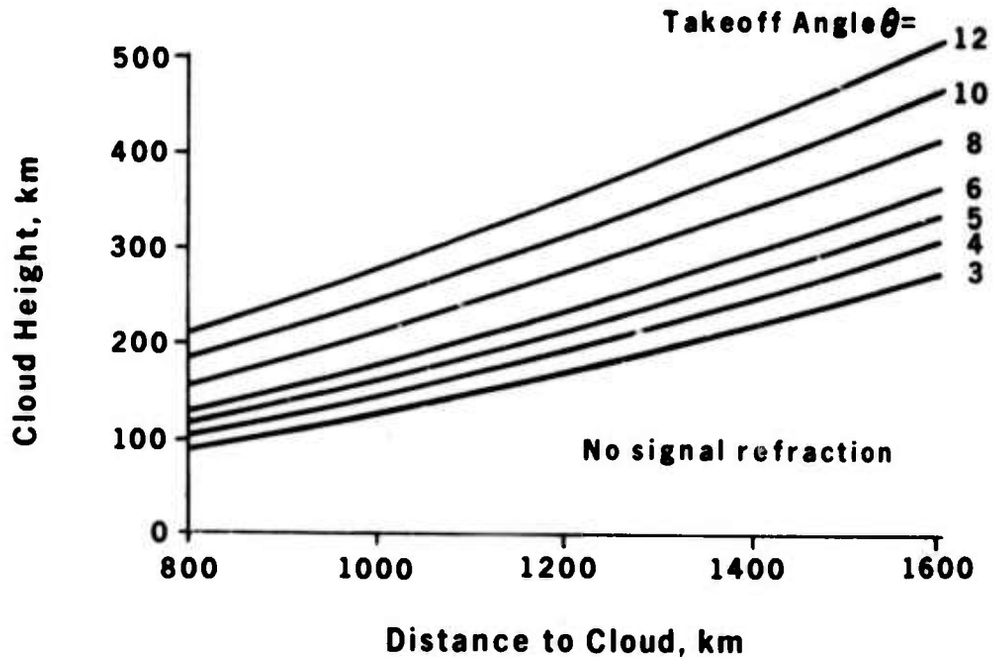

Figure 4-3. Relationship Between Cloud Height and Takeoff Angle vs Distance to Cloud Assuming No Signal Refraction.

estimating take-off angles required for various cloud heights and distances from the heater. This figure does not account for ionospheric or tropospheric signal refraction which could add 1-3 degrees to the takeoff angle.

4.4 EFFECTS OF SIGNAL FADING

Utilizing Figures 3-1 and 3-3, it is possible to obtain a feel for the problems to be encountered by deep signal fades. Figure 4-4 presents an estimate of the mean duration of fades below -20 dB from the median signal level. (Figure 3-1 shows such fades will occur 0.7 percent of the time.) The figure shows that one should expect a noticeable error rate on non-diversity 100 wpm teleprinter data during daytime even under good propagation conditions. For example, at 35 MHz, Figure 3-1 predicts 10 deep fades per minute which, according to Figure 4-4 would last 42 msec (creating a high probability of errors on two characters at a time). This implies a character error rate (CER) of at least 3 percent. Similar logic indicates a CER of at least 5 percent at 50 MHz. Both of these CER values are consistent with the measurements made during good propagation conditions in STEEP CLIFF I (see Reference 9).

Figure 4-4 also indicates that the CER of 100 wpm teleprinter data should be lower at nighttime than daytime for the same received signal-to-noise ratio due to the lower probability of fades affecting more than one character at a time. This expectation was confirmed during STEEP CLIFF II when non-diversity CER measurements as low as 1.8 percent were observed on 50 MHz.

4.5 EFFECTS OF DIVERSITY RECEPTION

The application of diversity reception techniques will help to compensate for the signal fading observed on cloud-scatter circuits. The effects of polarization, frequency, and space diversity have been examined.

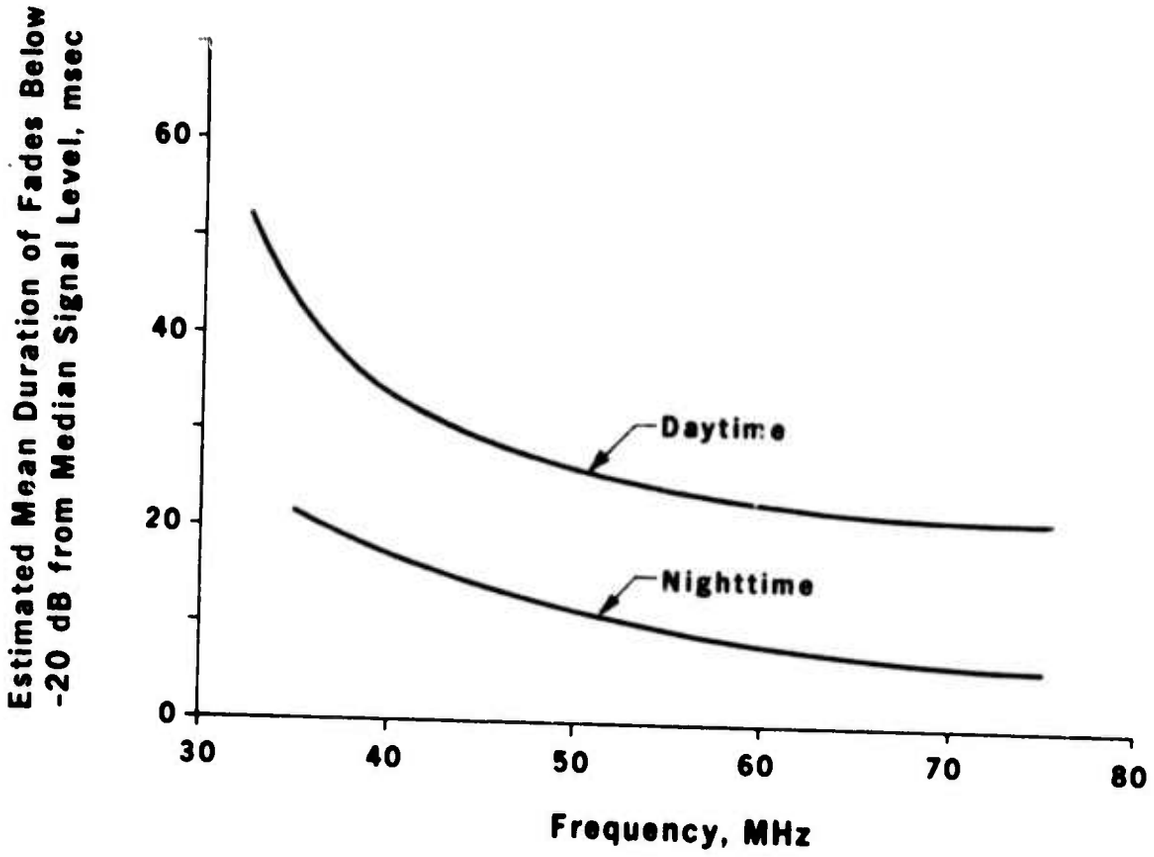

Figure 4-4. Estimated Mean Duration of Fades Below -20 dB from Median Signal Level vs Frequency.

The least successful technique is polarization diversity. The correlation coefficient resulting from the simultaneous measurement of output signal amplitudes from two fixed gain receivers, one connected to a vertically-polarized antenna and the other to a horizontally-polarized antenna, was found to be 0.44 (see Ref. 9).

Figure 3-4 suggests the requirements for frequency diversity. The measurements show that data separated by at least 3 kHz should be decorrelated.

Figure 4-5 shows the effects of space diversity for horizontally polarized receiving antennas. The figure presents the mean correlation coefficient of simultaneous signal amplitudes from two fixed gain receivers connected

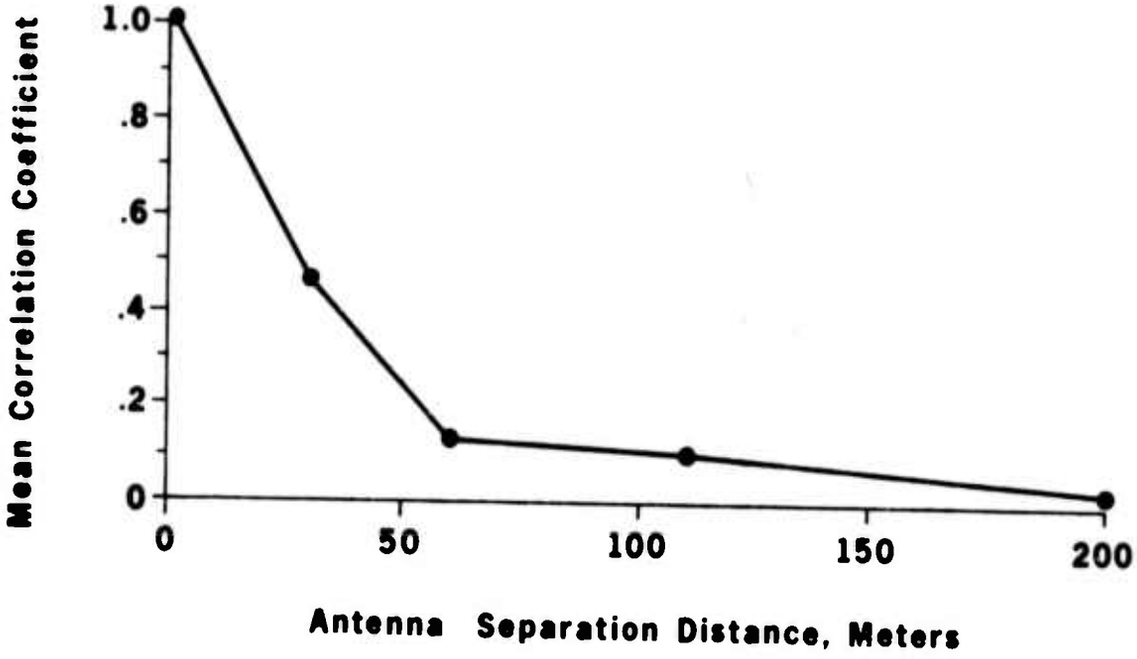

Figure 4-5. Mean Correlation Coefficient of Simultaneous Received Signal Level from Two Horizontally Polarized Antennas vs Separation Distance.

to antennas of varying separation distances. The signal levels are quite decorrelated for separation distances beyond about 60 meters.

The effect of diversity reception on teleprinter character error rate can be estimated by observing that if the best probability of a character error is 6% for a single channel in daytime, the best joint probability of two channels yielding a character error must be on the order of 0.4 percent. Figure 4-6 shows the effect of diversity combining two channels with CER's of 5.7 and 6.1 percent, respectively, yielding a CER of 0.8 percent. The CER improvement of the diversity-combined channel might have been greater had it not been for the occurrence of a thunderstorm near the receiver site during the test.

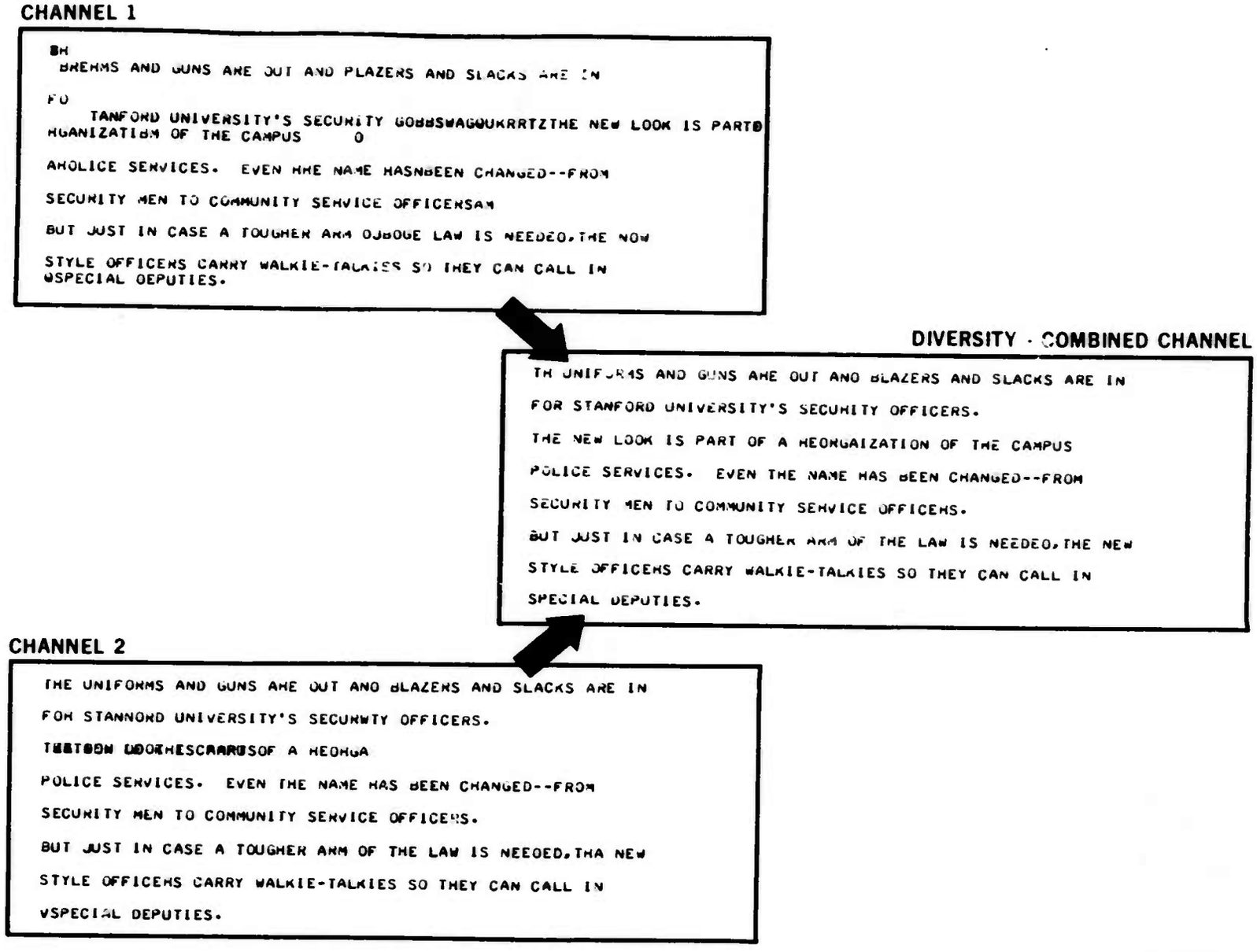

Figure 4-6. Example 100-wpm FSK Teleprinter Data Received During Daytime on 50 MHz Using Space Diversity Reception.

During nighttime, diversity combining two channels would be expected to yield even better results. If the probability of a CER with a single channel approaches 2 percent, the diversity-combined channel should approach the order of .04 percent. Figure 4-7 shows example teleprinter data for nighttime reception of channels with CER's of 2.8 and 1.8 percent respectively. Though no errors show in the figure for the diversity combined channel using antennas with 110-meter spacing, a CER of 0.05 percent was obtained during the entire test.

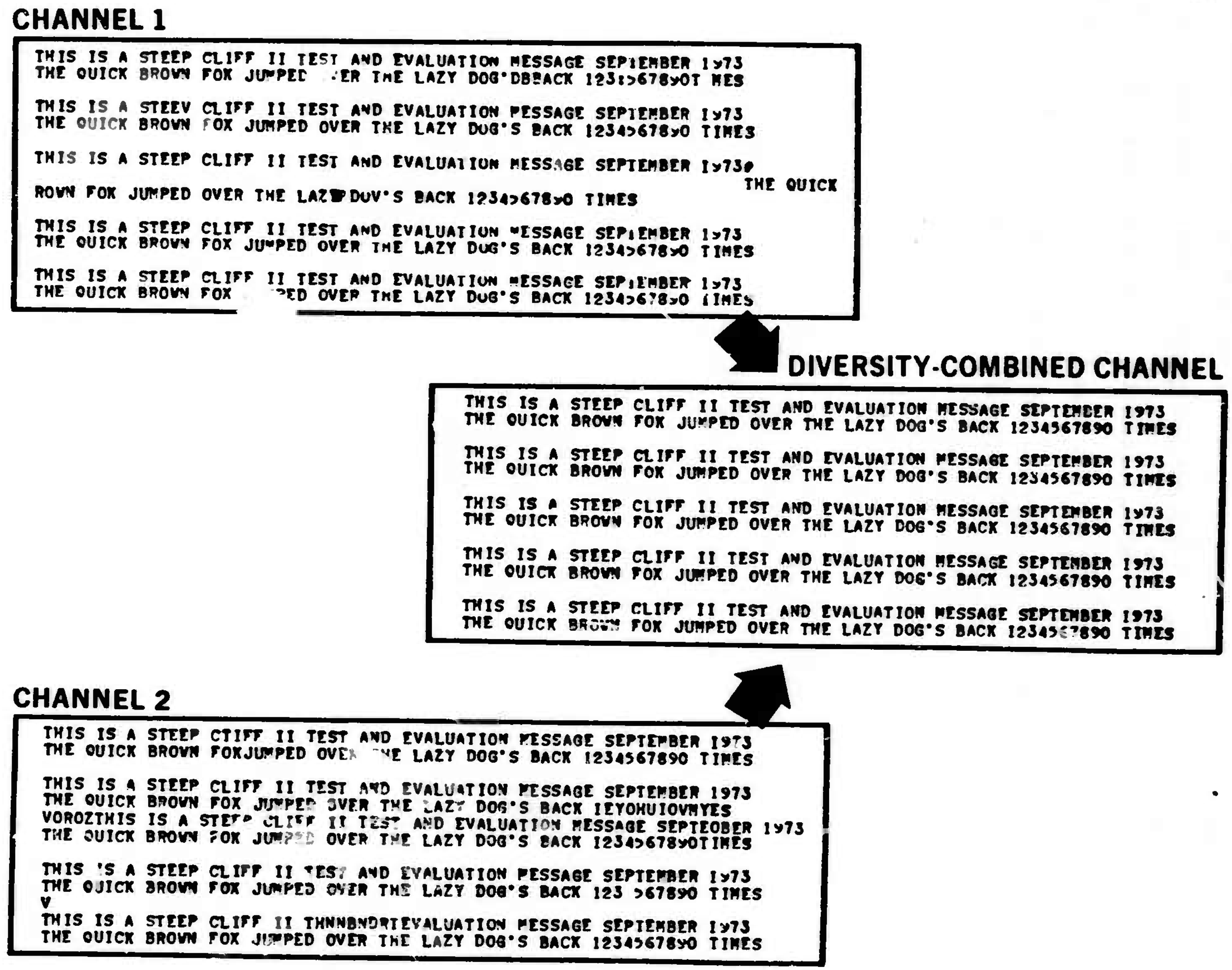

Figure 4-7. Example 100-wpm FSK Teleprinter Data Received During Nighttime on 50 MHz Using Space Diversity Reception.

Appendix A
Project STEEP CLIFF

Project STEEP CLIFF was a program of field experiments demonstrating long-range VHF communication applications using signal scatter off a man-made ionospheric "cloud" over Platteville, Colorado. The effort was divided into two parts which are described in the following discussion.

A.1 STEEP CLIFF I

STEEP CLIFF I consisted of two field experiments conducted in the summer and fall of 1972. The first field experiment was a communications demonstration in August 1972 that had two principal objectives:

1. Ascertain if voice and data could be transmitted over a beyond-the-horizon circuit employing the cloud-scatter technique; and

2. Determine the extent to which the technique decreased such a circuit's vulnerability to standard signal direction-finding (DF) methods.

Transmissions were made at 30 and 50 MHz on a 2178 km circuit from Katy, Texas, to Lancaster, California (see Figure A-1). Transmissions were made at 30 and 50 MHz consisting of voice (using single sideband modulation and FM), 1200 and 2400 bps data (using a Collins airborne-type data modem system), commercial FM facsimile, and 100 wpm FSK teleprinter data (nonsynchronous and synchronous). An FRD-10 DF system at Imperial Beach NAS, California, attempted to measure the direction of the transmitting source on 30 MHz.

In addition to the data transmissions, VHF oblique-incidence soundings were made. The soundings were used to establish the optimum cloud heights for the two transmission frequencies and to clearly show all modes

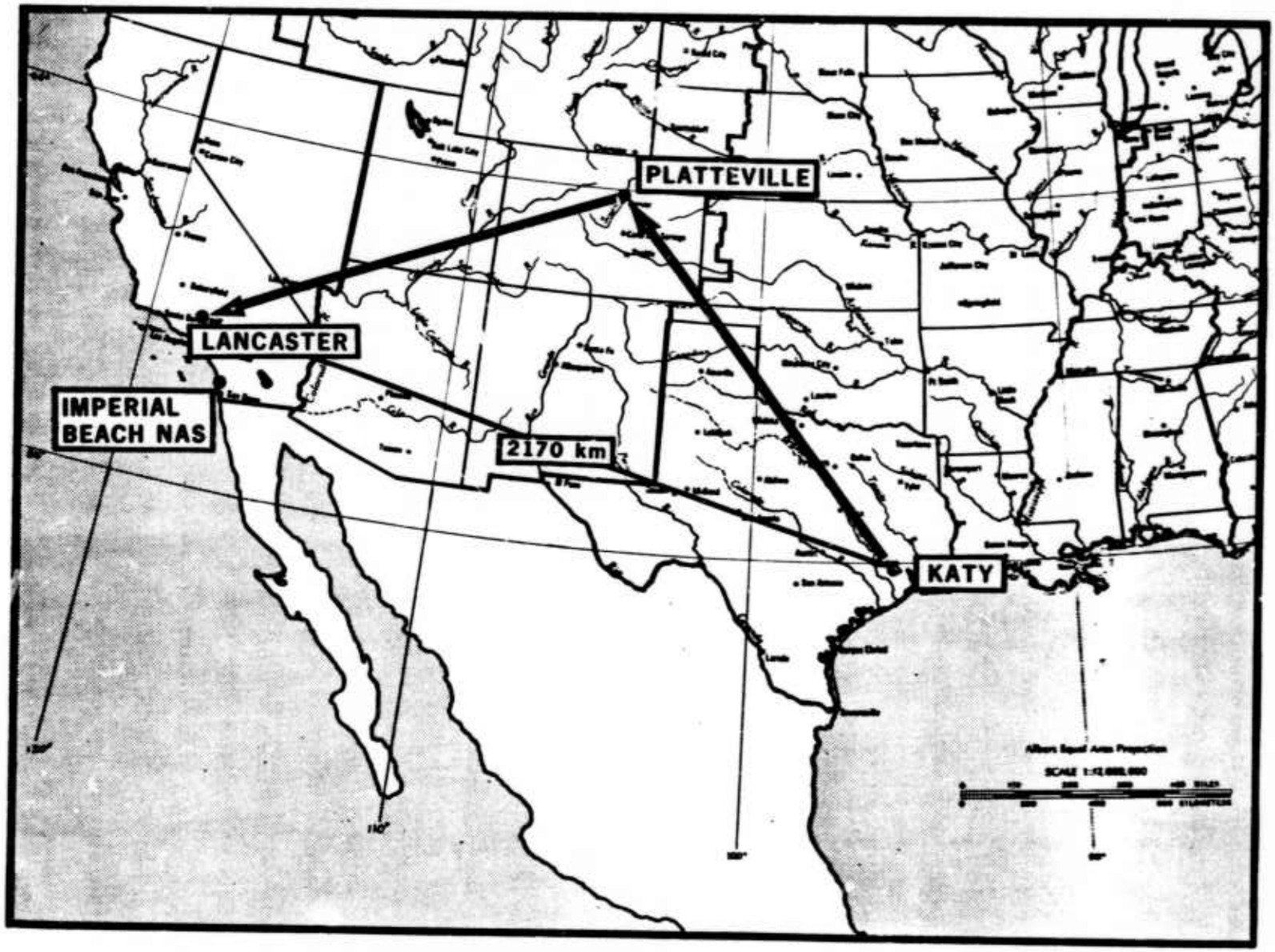

Figure A-1. STEEP CLIFF I Circuit Path.

of signal propagation between the two sites. The soundings were made using a Chirpsounder FM/CW system sweeping from 27.5 to 52.5 MHz in ten minutes. The sweep format provided a facsimile record of relative signal time delay as a function of frequency. The sounder record also plotted received signal-plus-noise and noise power in a 100 Hz bandwidth (dB vs frequency).

Additional tests were conducted over the same circuit in October 1972. These measurements were made to:

(1) Determine the effect on the observed scatterer cross-section as the heater transmitter power was varied; and

(2) Determine amplitude correlation of two signals as a function of their frequency separation and as received on two antennas of different polarization and spacing.

The experiment procedure and results of the STEEP CLIFF I field test program are discussed in detail in Reference 9. The test results form an important part of the conclusions presented in Sections 2, 3, and 4.

A.2 STEEP CLIFF II

The STEEP CLIFF II experimental program was performed in the autumn of 1973 with two objectives:

(1) To develop procedures for maintaining maximum cross section of the heated volume despite diurnal and seasonal ionospheric variations at the heater location; and

(2) To investigate the effects on observed cross section and received signal characteristics of varying heater power level and modulation.

To accomplish these objectives, the STEEP CLIFF transmitter site was moved from Katy to Del Rio on the Texas-Mexico border and a second

receiver site was built at Ocotillo, close to the California-Mexico border. The transmitter was relocated to maximize the received signal at night when a higher cloud (in the vicinity of 300 km) would be inevitable.

Figure A-2 shows the STEEP CLIFF II circuit paths. Contours are shown across California and Arizona where signals from a Del Rio transmitter would scatter to the ground from a field-aligned reflector at heights of 240, 270, and 300 km in the absence of ionospheric reflection.

To explore the frequency range from 30-120 MHz, an array of log periodic antennas were constructed. Figure A-3 shows the installation at Lancaster. Similar arrays were constructed at the other two sites.

Figure A-4 shows a block diagram of the equipment items used. As with STEEP CLIFF I, the equipment included a VHF oblique ionosonde system and fixed frequency transmission equipment. Two receivers for diversity reception and spectrum analyzer assembly, for observation of signal spectra and measurements of signal strengths in a wide range of selectable bandwidths, were the key receiving systems.

A.3 PERIODS OF DATA COLLECTION

As shown in Figure A-5, data was collected primarily during daylight hours in the 1972 STEEP CLIFF I experiments. Operating hours were staggered around the clock in the 1973 STEEP CLIFF II experiments.

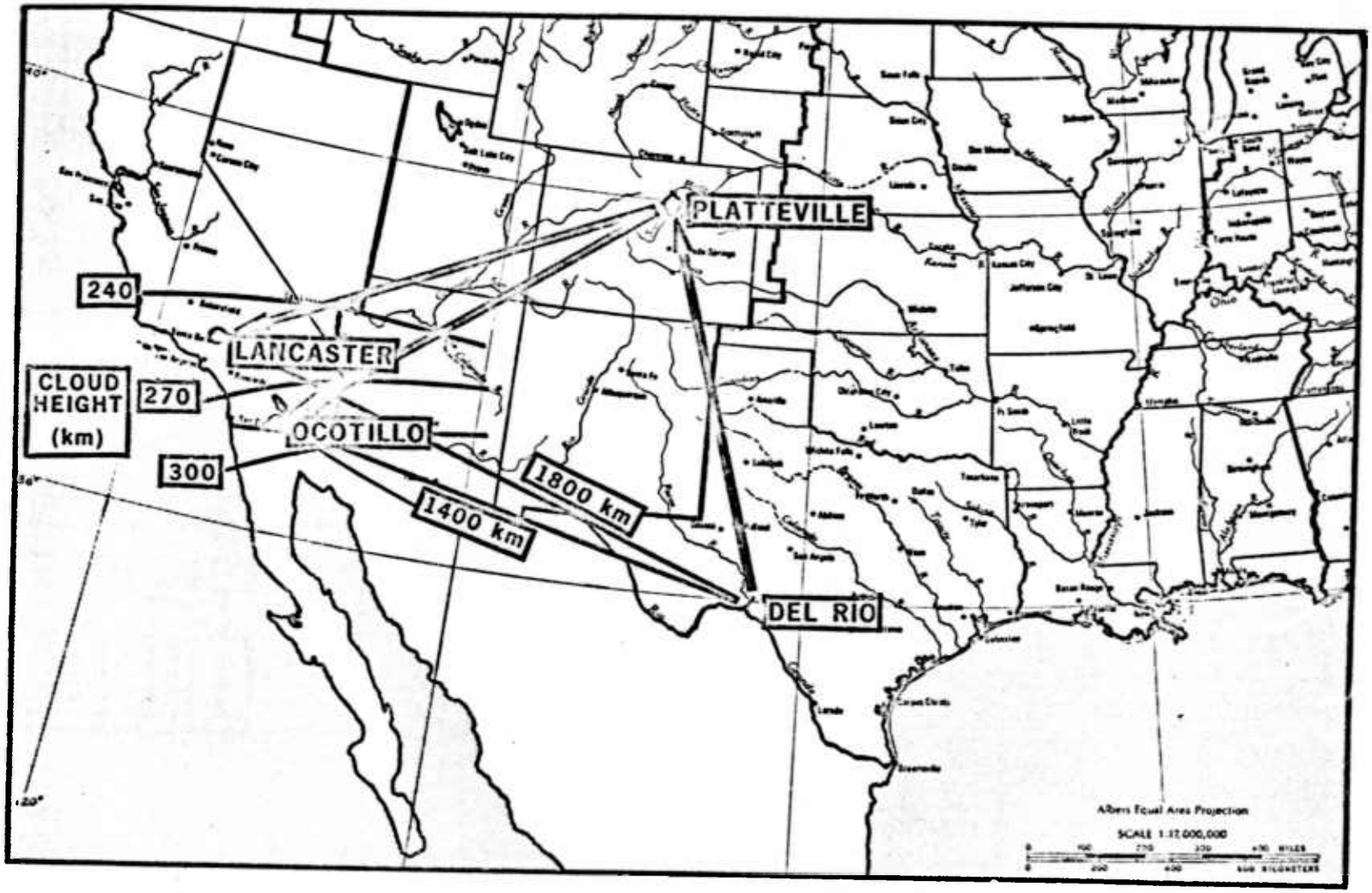

Figure A-2. STEEP CLIFF II Circuit Paths.

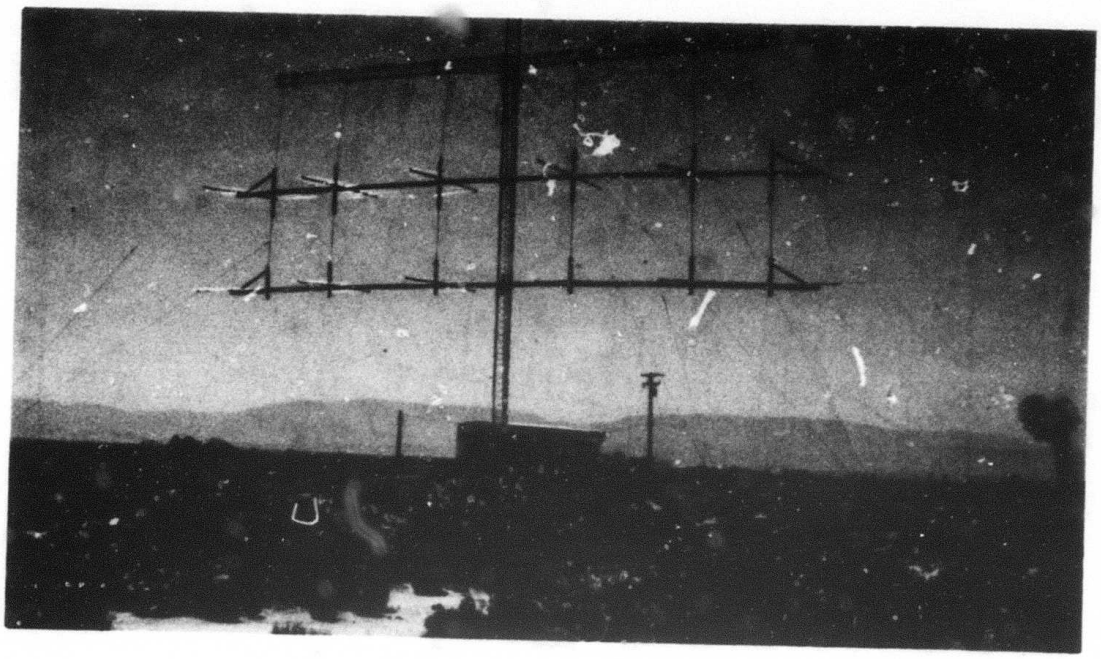

Figure A-3. Receiver Site at Lancaster, California.

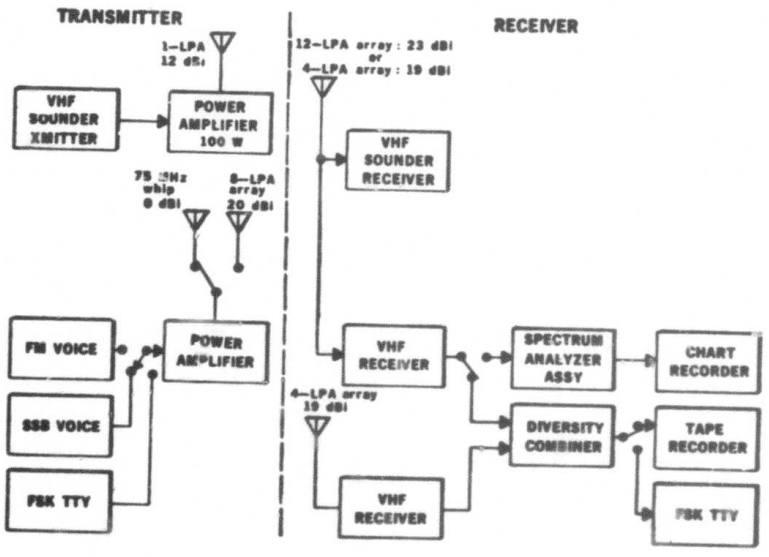

Figure A-4. Block Diagram of STEEP CLIFF II Equipment.

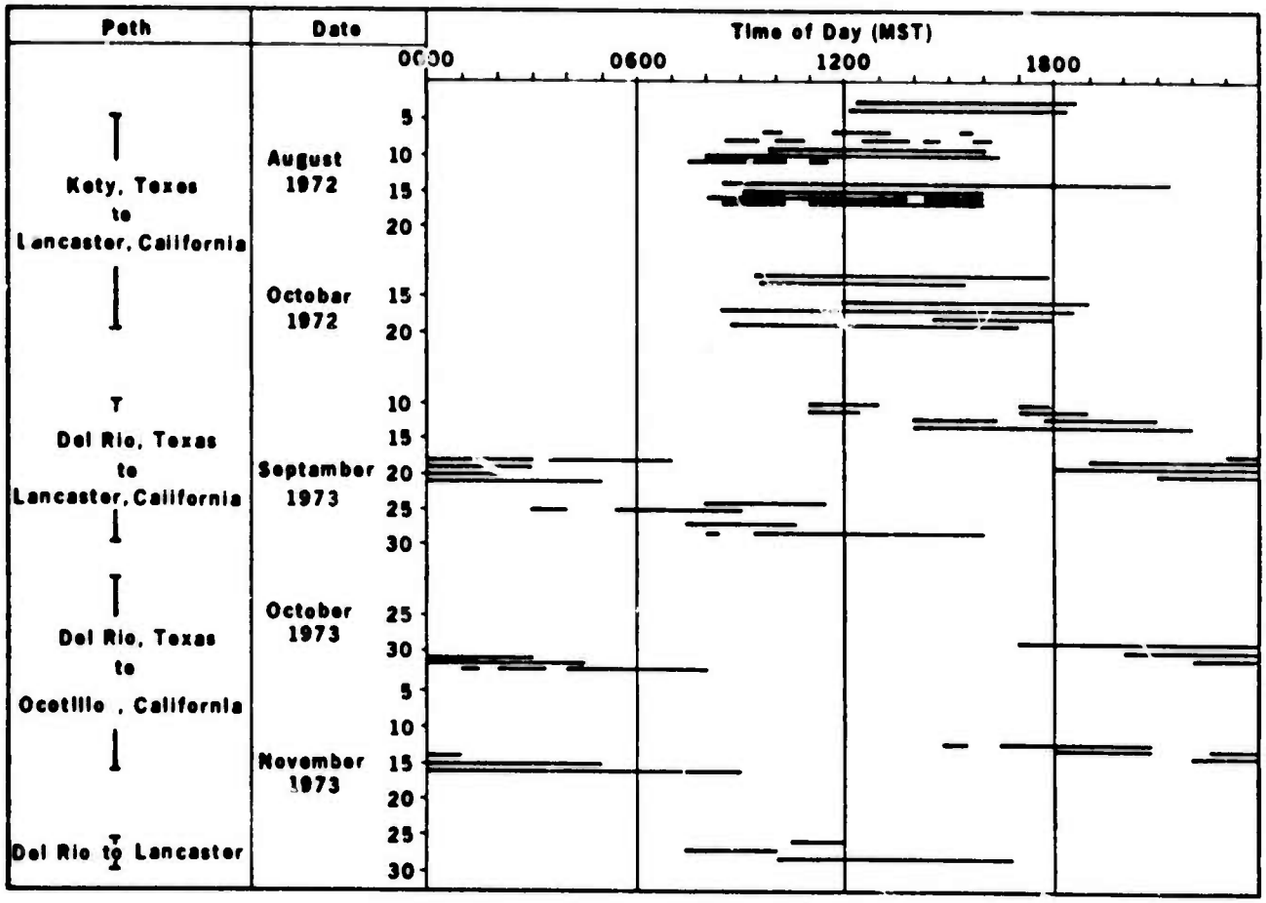

Figure A-5. Hours of Data Collection During 1972 Steep Cliff I and 1973 Steep Cliff II Experiments.

Appendix B

SUPPORTING DATA FOR FIGURES IN REPORT

The figures presented in Sections 2, 3, and 4 represent the result of a significant data collection effort. However, there are limitations inherent in nearly every figure and in order to apply the information contained in them, one must understand these limitations.

The data base for Project STEEP CLIFF consists of a little over two weeks data collection during August 1972, one week in October 1972, and six weeks spread through September, October, and November 1973. Each week rarely resulted in more than 40 hours of collection time. Although multiple transmitter and receiver locations were used, only the Platteville heater was employed.

The following section presents a brief summary of the data base and, in some cases, the experiment procedure resulting in each figure. The discussion is divided by the Sections 2, 3, and 4 in which the figures appear.

B.1 FIGURES IN SECTION 2

Figure 2-3. Maximum observed radar cross section calculated from maximum S/N ratios observed on all ionogram records at each frequency indicated. Data base includes all STEEP CLIFF I and II ionograms (258 total hours) without regard to time-of-day transmitter or receiver location; calculation technique is described in Appendix C.

Figure 2-4. Peak, mean, and median radar cross section calculated from ionogram data (See Appendix C) taken during STEEP CLIFF I and II during periods when the Platteville heater was operated at essentially full CW output. Daytime path data includes only observations at Lancaster (from

Katy and Del Rio transmissions); nighttime path data is taken only from ionograms recorded at Ocotillo during STEEP CLIFF II. Number of data points per hour range from one (0300-0500 for 50 MHz and 0400, 0500, 0700, 0900 for 65 MHz daytime; all nighttime 65 MHz values except 0100 and 0400) to 11 (1700 and 2000 at 35 MHz daytime); mean number of data points per hour applicable to each curve:

	Daytime	Nighttime
35 MHz	4.5	3.7
50 MHz	3.9	3.1
65 MHz	2.8	1.0

Figure 2-5. Data points accumulated from six separate tests of relative cross section yield vs heater power conducted during STEEP CLIFF II daytime and nighttime as summarized in Table B-1. Heater power was regulated as shown in Figure B-1 and output levels were monitored closely. An alternate procedure for heater changing power level vs time (see Figure B-2) was also attempted and data recorded on three occasions. The data points also fell within the envelope shown. References 7 and 13 present additional data recorded during these tests.

Table B-1

EXPERIMENTS YIELDING DATA POINTS FOR FIGURE 2-5

Date	Start Time (MST)	Heater Freq. (MHz)	Nominal Max Heater Power (MW)	Diagnostic Freq. (MHz)
Sept. 10	1230	6.49	1.7	75
Sept. 18	2030	4.45	1.0	41
Sept. 18	2310	2.80	0.9	41
Sept. 19	2040	3.20	1.5	42
Sept. 19	2330	2.85	1.5	42
Sept. 28	1143	7.37	1.2	50

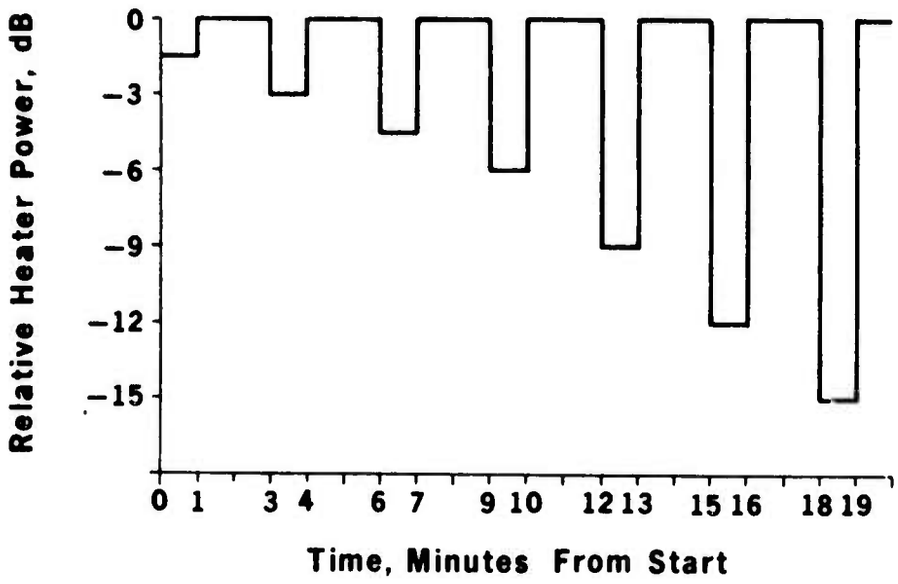

Figure B-1. Nominal Heater Power Level vs Time for Cross Section Yield Tests Used for Figure 2-5.

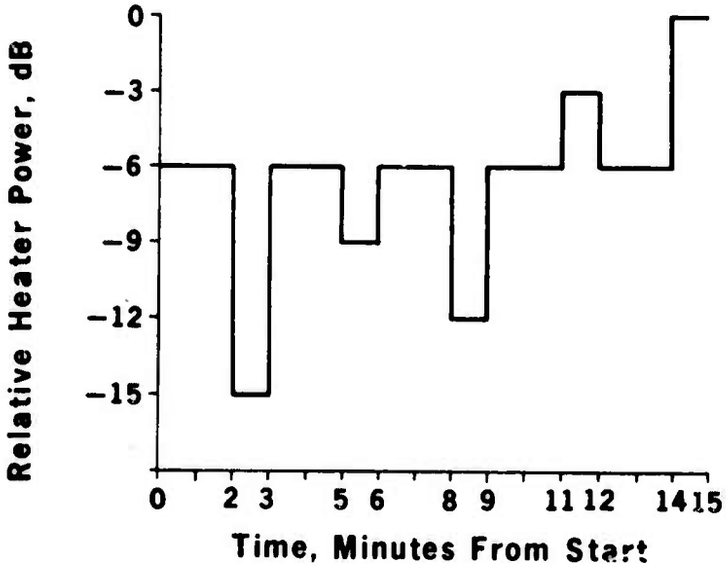

Figure B-2. Alternate Procedure for Heater Power Level vs Time.

Figure 2-6. Observed median relative radar cross section vs time obtained from received signals at various frequencies during periods of heater shut-down. Each daytime curve represents median of four separate measurements. The nighttime curve is from one measurement at the frequency noted, but additional measurements at other frequencies showed similar results.

Figure 2-7. Relative radar cross section observed on 16 November 1973 by pulsing heater at a 33 Hz rate with different duty cycles and power levels before and after sunrise. CW diagnostic signal at 40 MHz sent over Del Rio to Ocotillo circuit. Data corresponds to earlier finding during STEEP CLIFF I (see Ref. 9).

Figure 2-8. Relative median radar cross section observed on 29 November 1973 at approximately 1540 MST over Del Rio to Lancaster circuit using CW diagnostic signal near 41 MHz. Relative heater power comes from estimates by Platteville operators based on heater input power and may, therefore, be somewhat in error.

Figure 2-9. Ionograms shown in this figure were obtained during STEEP CLIFF I on 11 August 1972 circa 1630-1700 MST. See Reference 9 for further discussion.

Figure 2-10. Estimated plasma frequency above Platteville obtained by the Institute for Telecommunications Sciences, U. S. Department of Commerce, from true height profile analysis of vertical ionograms obtained on dates and times indicated in Figure.

Figure 2-11. Variation of observed cross section as the heater frequency was changed between limits shown. Data was collected on five separate nights during 1-16 November 1973 period over Del Rio to Ocotillo circuit. Various diagnostic signal frequencies were used in 40-50 MHz range.

Figure 2-12. Variation in radar cross section observed at 45 MHz on oblique sounder records following change in heater frequency associated with normal operation. Data base consisted of 70 measurements collected throughout STEEP CLIFF II on both circuits.

B.2 FIGURES IN SECTION 3

Figure 3-1. Fades per minute greater than 20 dB below median signal level scaled from recordings of signal amplitude vs time. Nighttime data points were obtained over Del Rio to Ocotillo circuit around 0100 MST on 1 November 1974. The daytime data represents a composite of measurements at 30 and 50 MHz over Katy-Lancaster circuit on 7 August 1972 around 1500 MST; at 41, 49, and 60 MHz over Del Rio-Lancaster circuit on 29 November 1973 around 1630 MST; and at 75 MHz over the same circuit on 10 September 1973 around 1300 MST. Thus, daytime seems independent of path, season, and year.

Figure 3-2. Facsimile recordings made during STEEP CLIFF I and obtained from Reference 9. Data represents typical output that could be expected under good propagating conditions.

Figure 3-3. Signal strength distribution obtained by scaling received amplitude vs time recordings. The daytime data was collected over the Del Rio to Lancaster circuit on 29 November 1973, while the nighttime data was obtained on the Del Rio to Ocotillo circuit 1 November 1973. The same recordings were part of the data base for Figure 3-1.

Figure 3-4. Correlation coefficient of signal amplitudes obtained simultaneously on two receivers tuned to separated frequencies. Each point on a curve represents the correlation coefficient of approximately 60 samples. The "good" daytime curve represents the highest correlation coefficient vs Δf observed and was obtained on the Katy-Lancaster circuit on October 1972 (see Ref. 9). The nighttime curve represents the best and worst correlation

observed on six separate tests over the Del Rio to Ocotillo circuit on 29 October, 14 November, and 15 November 1973.

Figure 3-5. Scatter plot of the estimated Δf at which the correlation coefficient was 1/e vs relative time delay spread observed on the oblique ionograms at the diagnostic nominal signal frequency. The seven data points represent all the day and night series of experiments used to obtain Figure 3-4.

Figure 3-6. STEEP CLIFF II ionograms showing daytime propagation over most of the 30-80 MHz range. Observed signal propagation above 70 MHz was the exception rather than the rule.

Figure 3-7. Variation of relative total time delay vs frequency observed on STEEP CLIFF II ionograms recorded at Lancaster during those periods of full power heater CW operation. The number of data points at each frequency and time (within ±30 minutes) is indicated.

Figure 3-8. The reciprocal of the relative time delay vs time of day at the heater obtained from ionograms recorded on the STEEP CLIFF II circuit to Lancaster only during those periods of full power CW operation by the heater. This is the same data base used to obtain Figure 3-7.

Figure 3-9. Typical mean signal spectra obtained by scaling photographs of spectrum analyzer output. The "nighttime" plot was obtained by computing the mean signal-plus-noise power vs frequency from four spectrum samples obtained at Ocotillo on 30 October 1973 around 2200 MST. The "daytime" plot represents the mean spectra from two samples obtained at Lancaster on 28 November 1973 around 1530. In total over 60 separate recordings of signal spectra were obtained during STEEP CLIFF I and II, and the general characteristics of these samples resembled those shown in Figure 3-9.

Figure 3-10. A replot of the data used for Figure 3-9 to show percent of signal power vs bandwidth surrounding the received carrier.

Figure 3-11. A composite plot of signal-plus-noise to noise spectra of a 40-MHz CW signal observed at Ocotillo on 16 November 1973 at approximately one hour intervals between 0430 and 0730 MST. The mean power in 2-Hz cells was scaled from photographs of spectrum analyzer output and ratioed to the mean noise floor to obtain the plots.

Figure 3-12. Frequency vs time of the peak signal level and the -20 dB power levels from eight spectra observations at Ocotillo on 30 October 1973 between 2150 and 2850 MST. A 41-MHz CW signal was spectrum analyzed with approximately 0.4 Hz resolution to obtain the data shown.

B.3 FIGURES IN SECTION 4

Figure 4-1. A plot of equation (4-2) expressed in logarithmic terms using the values quoted in the text.

Figure 4-2. A plot of equation (4-2) expressed in logarithmic terms using the lowest observed median cross section vs frequency from Figure 2-7 and adjusting this value assuming Rayleigh signal distribution as given in Figure 3-3.

Figure 4-3. A plot of the equation

$$H = \sqrt{R^2 + d^2 - 2Rd \cos(90 + \theta)} - R$$

where H = cloud height, km

d = straight line distance to cloud, km

θ = takeoff angle, deg

R = radius of earth = 6,375 km

Figure 4-4. Estimated mean duration of fades exceeding -20 dB from the median signal level. From the assumption of Rayleigh signal distribution,

fades exceeding -20 dB occur 0.7 percent of the time or 420 msec/minute. Figure 3-1 was then used to obtain the number of such fades per minute for calculating their mean duration.

Figure 4-5. Mean correlation coefficients computed from a series of observations at Lancaster taken during the STEEP CLIFF program. Table B-2 presents the data base used.

Table B-2

DATA BASE FOR FIGURE 4-6

Separation Dist., m	Date	Time, MST	T-Site	Freq, MHz	No. of Samples	Correl. Coeff.	Mean Cor. Coeff.
30	18 Sept 73	0930	Del Rio	50	59	.421	.469
	"	0940		50	60	.304	
	"	0950		50	59	.682	
60	25 Sept 73	0900	Del Rio	50	64	.204	.123
	"	0905		50	62	.013	
	27 Sept 73	0810		50	59	.153	
110	18 Sept 73	2119	Del Rio	41	52	.010	.107
	"	2120		41	69	.203	
200	19 Oct 72	1505	Katy	50	35	.006	.006

Figure 4-6. Example of 100 wpm teleprinter data during daytime on 50 MHz with space diversity obtained 19 October 1972 during STEEP CLIFF I. Antenna separation was 200 meters.

Figure 4-7. Example of 100 wpm teleprinter data during nighttime on 50 MHz with space diversity of 110 meters obtained 19 September 1973 during STEEP CLIFF II.

Appendix C

PROCEDURE FOR CROSS SECTION CALCULATION

Section 2 presents data regarding observed cross section of the ionospheric disturbance volume created above Platteville. The cross sections were calculated from the VHF oblique sounder data by the method described in the following section.

C.1 BASIC RELATIONSHIPS

The effective observed cross section is obtained from the oblique ionosonde data from the following relationship:

$$\sigma = \frac{(4\pi)^3 R_T^2 R_R^2 (SNR) P_N}{P_T G_T G_R \lambda^2} \qquad \text{(C-1)}$$

where R_T = distance from transmitter to cloud, meters

R_R = distance from cloud to receiver, meters

SNR = signal-to-noise ratio in receiver bandwidth

P_N = noise power in receiver bandwidth

P_T = sounder transmitter power, watts

G_T = transmitting antenna gain

G_R = receiving antenna gain

λ = wave length, meters

The oblique ionosonde provides a direct measure of received noise power, N in dBW, and signal-plus-noise power S + N in dBW, vs frequency. Signal-

to-noise ratio (SNR), in dB, is obtained from these measurements by the relationship.

$$(SNR)_{dB} = 10 \log \left[10^{(S+N)-N} - 1\right] \qquad (C-2)$$

Noise power in a 100-Hz bandwidth was obtained in values of dBm by using a calibrated noise source within the sounder receiver. The bottom of the power graph associated with the ionogram (see Figure 2-10) was set at -177 dBW. Therefore, actual noise power at the antenna was obtained from the relationship

$$P_N = -177 + N - L_R(f) \qquad (C-3)$$

where $L_R(f)$ was the loss in dB as a function of frequency within the antenna system (e.g. pre-amp gain, coax attenuation).

In computing total gain for the horizontally polarized sounder antennas, one must recognize that total field strength is given by

$$E_T = E_i \left[1.0 + R_h e^{-j(\frac{4\pi h}{\lambda} \sin \Delta)}\right] \qquad (C-4)$$

where E_i = incident field strength

R_h = complex horizontal polarization reflection coefficient

h = antenna height

λ = wave length

Δ = signal takeoff angle

For purposes of estimating antenna gain, one can evaluate eq (C-4) relative to an isotropic antenna and express the square of the resulting ratio in the form

$$G(f) = G_{fs}(f) + G_{ref} + 10 \log \left| 1 - \cos \left(\frac{4\pi h}{\lambda} \sin \Delta \right) \right| \qquad \text{(C-5)}$$

where $G_{fs}(f)$ is the free space gain as a function of frequency, in dBi, of the antenna array and G_{ref} is the reflection gain dependent on the ground characteristics in the Fresnel zone. If the ground were a copper sheet G_{ref} would be 3 dB. However, for VHF signals above 30 MHz, takeoff angles less than 10 degrees, and for generally dry poor conducting ground, G_{ref} remains fairly independent of frequency and assumes typical values of 0 to 2 dB. A value of 1 dB was assumed in all calculations. Coax attenuation within the transmitting antenna system was considered part of the quantity G_{fs}.

Substituting equations (C-2), (C-3), and (C-5) into (C-1) in logarithmic form and simplifying yields:

$$\begin{aligned} \sigma = & -146 + 20 \log R_T + 20 \log R_R + 10 \log (10^{(S+N)-N} - 1) + N \\ & - L_R(f) - 10 \log P_T - G_{fsT}(f) - 10 \log \left| 1 - \cos \left(\frac{4\pi h}{\lambda} \sin \Delta \right) \right|_T \\ & - G_{fsR}(f) - 10 \log \left| 1 - \cos \frac{4\pi h}{\lambda} \sin \Delta \right|_R - 20 \log \lambda \end{aligned} \qquad \text{(C-6)}$$

which places σ in a form using only measured or, in the case of takeoff angle Δ, estimated quantities. This equation can be further simplified into the form

$$\sigma = A(f) + N - (SNR)_{dB} \quad (\text{dBsm}) \qquad \text{(C-7)}$$

where A(f) is determined for each path and cloud height, N is directly measured from the sounder data, and (SNR) is computed from the measure of (S + N)-N from the sounder data. Of course, if (S + N)-N is 10 dB or greater, then equation (C-7) is approximated by $\sigma = A(F) + (S + N)$.

C.2 CROSS SECTION COMPUTATION

Table C-1 summarizes the values used in the computation of A(f) from eq. (C-7) for the Katy-Lancaster circuit used in STEEP CLIFF I. A 1000-watt transmitter and an LPA array were employed.

For STEEP CLIFF II, the computation of A(f) becomes more complicated as several antenna arrays were used and operations ran both day and night. During daytime, cloud heights of 240-250 km were typical; at night, typical heights were in the 290-300 km range.

The term A(f) in eq. C-7 can be divided into three parts:

$$A(F) = A_o(f) - G_T(f) - G_R(f) \qquad (C-8)$$

where $A_o(f) = -146 + 20 \log R_T + 20 \log R_R - 10 \log P_T - 20 \log \lambda$

$$G_T(f) = G_{fsT}(f) + 10 \log \left| 1 - \cos \left(\frac{4\pi h}{\lambda} \sin \Delta \right) \right|_T$$

$$G_R(f) = G_{fsR}(f) + 10 \log \left| 1 - \cos \left(\frac{4\pi h}{\lambda} \sin \Delta \right) \right|_R + L_R(f)$$

Table C-2 presents the values used to compute $A_o(f)$ for the STEEP CLIFF II circuits. Del Rio, Lancaster, and Ocotillo were essentially the same distance from Platteville (approximately 1200-1300 km).

Table C-3 summarizes the $G_T(f)$ values computed for Del Rio. The transmitting antenna system consisted of an array of 3 rows of four 30-120 MHz LPA antennas, with the rows at approximately 7, 11, and 15 meters height, and two 30-90 MHz single LPA antennas at 7 and 11-meter elevations. Figure C-1 shows the measured gain of these antennas; note the drop in measured gain of the 30-120 MHz antenna in the 50-85 MHz range. The rows of 30-120 MHz LPA's were either used singly or in pairs (upper two and lower two rows).

Table C-1

Values Assumed for Computation of Cross Section
for Katy-Lancaster Circuit
(STEEP CLIFF I)

Item	Frequency, MHz				
	30	35	40	45	50
$20 \log R_T$	123				
$20 \log R_R$	122				
$L_R(f)$	21				
P_T	30				
$G_{fsT}(f) = G_{fsR}(h)$	11	12	12	12	12
$\frac{h_T}{\lambda} = \frac{h_R}{\lambda}$ (h = 10.35 m)	1.035	1.208	1.380	1.552	1.725
Δ_T (deg) for 240 km cloud	6.0	5.7	5.5	5.3	5.1
$10 \log \left\lvert 1 - \cos \left(\frac{4\pi h}{\lambda} \sin \Delta\right)\right\rvert_T$	-1	-1	-1	0	0
Δ_R (deg) for 240 km cloud	5.5	5.2	5.0	4.8	4.6
$10 \log \left\lvert 1 - \cos \left(\frac{4\pi h}{\lambda} \sin \Delta\right)\right\rvert_R$	-1	-1	-1	0	0
$20 \log \lambda$	20	19	18	16	16
A(f)	8	7	7	7	7

Table C-2

Values Used to Compute $A_o(f)$ for STEEP CLIFF II Circuits

Item	Frequency, MHz						
	35	40	45	50	55	65	75
20 log R_T	122						
20 log R_R	122						
10 log P_T	20	20	19	18	18	17	17
20 log λ	19	18	16	16	15	13	12
$A_o(f)$	59	61	63	65	66	68	69

Table C-3

Values Used for $G_T(f)$ of Del Rio
Transmitter Site in STEEP CLIFF II

Item	Frequency, MHz						
	35	40	45	50	55	65	75
Δ (daytime)	8.0	7.4	7.0	6.7	6.4	6.2	6.0
$G_T(f)$ for top 1 x 4 LPA array	18	18	18	19	15	15	13
$G_T(f)$ for upper 2 x 4 LPA array	20	21	21	21	18	19	18
$G_T(f)$ for upper single LPA	10	10	10	11	11	10	8
$G_T(f)$ for lower single LPA	7	7	8	8	9	9	10
Δ (nighttime)	10.5	10.0	9.5	9.0	8.6	8.2	8.0
$G_T(f)$ for top 1 x 4 LPA array	17	17	16	15	11	6	-9
$G_T(f)$ for middle 1 x 4 LPA array	18	18	19	19	15	15	14
$G_T(f)$ for lower 2 x 4 LPA array	20	20	21	21	18	19	18
$G_T(f)$ for upper single LPA	11	11	11	11	11	10	8
$G_T(f)$ for lower single LPA	9	9	10	10	10	10	11

At the Lancaster and Ocotillo receiving sites, arrays of LPA's consisting of two rows of six antennas were constructed. The two rows at Lancaster were at 11 and 15 meters elevation, while the rows at Ocotillo were 6 and 11 meters above ground. Table C-4 summarizes the resulting $G_R(f)$ values for the associated signal take-off angles indicated.

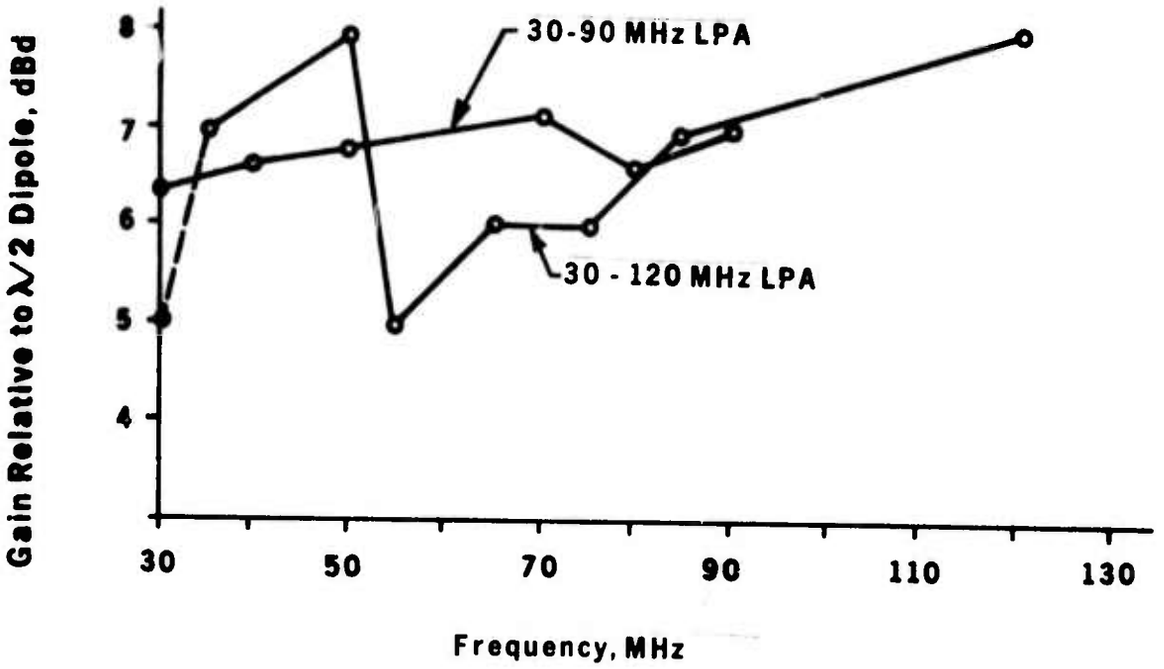

Figure C-1. Measured Gain of LPA Antennas Used During STEEP CLIFF II.

Table C-4

Values Used for $G_R(f)$ for STEEP CLIFF II
Receiver Sites

Item	Frequency, MHz						
	35	40	45	50	55	65	75
Δ (daytime), deg	5.5	5.2	4.9	4.7	4.6	4.5	4.5
Δ (nighttime), deg	8.0	7.7	7.4	7.0	6.8	6.6	6.5
$G_R(f)$ - Lancaster							
Daytime	14	15	15	16	13	14	15
Nighttime	16	16	16	16	13	14	12
$G_R(f)$ - Ocotillo							
Daytime	11	12	13	13	11	13	13
Nighttime	14	14	15	16	13	14	14

Table C-5

Values Used for A(f) in Computation of Cross Section for
STEEP CLIFF II

Rcvr Site	Transmitting Antenna System	Frequency, MHz													
		Daytime							Nighttime						
		35	40	45	50	55	65	75	35	40	45	50	55	65	75
L	Top 1 x 4 array	3	4	6	7	14	15	18	3	4	7	9	18	24	42
	Middle 1 x 4 array	-	-	-	-	-	-	-	2	3	4	5	14	15	20
	Upper 2 x 4 array	1	1	3	4	11	11	13	-	-	-	-	-	-	-
	Lower 2 x 4 array	-	-	-	-	-	1	-	0	1	2	3	11	11	16
	Upper single LPA	11	12	14	15	18	19	20	9	10	12	13	18	20	23
	Lower single LPA	14	15	16	17	21	21	21	11	12	13	14	19	20	26
O	Upper 2 x 4 array	6	6	7	9	15	16	17	-	-	-	-	-	-	-
	Upper single LPA	16	17	18	20	22	25	25	13	14	14	16	20	24	26
	Lower single LPA	19	20	20	22	24	26	25	15	16	16	17	21	22	23

REFERENCES

(1) Ginzburg, V. L., and A. V. Gurevich, "Nonlinear Phenomena in a Plasma Located in an Alternating Electromagnetic Field," Sov. Phys. Usp., 3, pp 115-146 and 175-194, 1960.

(2) Stanford Research Institute, "Proceedings of Prairie Smoke I RF Measurements Data Workshop," SRI report 2-4335, March 1972.

(3) Stanford Research Institute, "Proceedings of Prairie Smoke II RF Measurements Data Workshop," SRI report 2-5388, October 1972.

(4) Stanford Research Institute, "Proceedings of Prairie Smoke III RF Measurements Data Workshop," SRI report 3-4068, January 1973.

(5) Stanford Research Institute, "Proceedings of Prairie Smoke IV RF Measurements Data Workshop," SRI report 3-4836, June 1973.

(6) Stanford Research Institute, "Proceedings of the Ivory Coral 1973 Technical Review Meeting," SRI reports 3-4533 (Vol. I: Theory) and 3-4534 (Vol. II: Experiments), April 1973.

(7) Stanford Research Institute, "Proceedings of the Prairie Smoke V RF Measurements Workshop," November 1973.

(8) Vanderlind, M. R., "A Technical Summary of the Ivory Coral Program on Ionospheric Modification," compiled and edited at Battelle Columbus Laboratories, published by Stanford Research Institute, 11 March 1974.

(9) The Mitre Corporation, "Communication via a Modified Ionosphere," Mitre Document M73-87, 5 April 1973.

(10) This reference is available to qualified military and government agencies on request from RADC (OCSE) Griffiss AFB NY 13441.

(11) Arnold, Pitt W., "An HF High-Power Vertically Directed Array for Ionospheric Modification," U.S. Department of Commerce OT Report 73-21, October 1973.

(12) McNamee, C. M., and Woodbury, R. S., "A Nomogram for Bistatic Ivory Coral Experimenters," Barry Research Corp., document 746-72, September 1972.

(13) Minkoff, J., et al., "RRI Prairie Smoke V Results," RRI Memorandum M-5/174-4-50, 7 January 1974.